SUPER-RESOLUTION ALGORITHM APPLIED TO SPECTRAL IMAGES ACQUIRED VIA COMPRESSIVE SENSING

HOOVER FABIAN RUEDA CHACÓN

UNIVERSIDAD INDUSTRIAL DE SANTANDER
FACULTY OF PHYSICAL-MECHANICAL ENGINEERING
SCHOOL OF SYSTEMS AND INFORMATICS ENGINEERING
BUCARAMANGA
2012

SUPER-RESOLUTION ALGORITHM APPLIED TO SPECTRAL IMAGES ACQUIRED VIA COMPRESSIVE SENSING

HOOVER FABIAN RUEDA CHACÓN

Thesis submitted in partial fulfillment of the requirements for the degree of:
Master of Science in Systems and Informatics Engineering

Director:
PhD(c), MPE. HENRY ARGUELLO FUENTES

UNIVERSIDAD INDUSTRIAL DE SANTANDER
FACULTY OF PHYSICAL-MECHANICAL ENGINEERING
SCHOOL OF SYSTEMS AND INFORMATICS ENGINEERING
BUCARAMANGA
2012

A Dios por la inteligencia, la sabiduría, el entendimiento y la serenidad para afrontar los retos de cada día, por la salud y todos los favores recibidos.

A mi mamita Cecilia por su apoyo, amistad y consejos, especialmente por su amor, comprensión y acompañamiento a lo largo de mi vida. Por sus enseñanzas, su nobleza, lucha y fortaleza para salir adelante.

A mi hermano Fernando por su apoyo incondicional, por ser la compañía en pasajes importantes de mi vida, siendo mi amigo y confidente.

A mi hermosa novia Claudia, por todo su amor, comprensión, apoyo, inteligencia, belleza y por su espectacular sonrisa, motivo de inspiración y olvido de dificultades. Por compartir sus ideales conmigo y dejarme ser parte de ellos.

A mi familia, por el entorno que me han otorgado, por el orgullo que siento de formar parte de ésta, por los valores inculcados y todo el apoyo dispensado.

A mi director , Profesor Henry Arguello por sus enseñanzas y por ser más que mi director, mi guía espiritual y motivo de lucha y dedicación para conseguir los objetivos.

Y a todas las personas que de una u otra forma han estado conmigo a lo largo de este camino.

Hoover

Contents

List of Figures

Resumen

TITULO: ALGORITMO DE SUPER-RESOLUCIÓN APLICADO A IMÁGENES ESPECTRALES ADQUIRIDAS MEDIANTE LA TÉCNICA DE COMPRESSIVE SENSING[1]

AUTOR: HOOVER FABIAN RUEDA CHACÓN [2]

PALABRAS CLAVE: Imágenes espectrales, super-resolución, compressive sensing, sistemas ópticos basados en aperturas codificadas

Los sistemas ópticos para la obtención de imágenes basados en aperturas codificadas se encuentran a la vanguardia del modelado óptico debido a que permiten capturar la información espectral de una escena tridimensional en una única medicion bidimensional, a diferencia de los instrumentos ópticos basados en ranuras que deben escanear la región completa línea por línea. El sistema de adquisición de imágenes espectrales basado en apertura codificada de única captura (CASSI) es una sobresaliente arquitectura óptica, la cual sensa la informacion spectral de una escena real utilizando los conceptos fundamentales de compressive sensing (CS). El objetivo de este trabajo es transformar escenas de alta resolución en señales comprimidas capturadas por detectores de baja resolución. Super-resolución espacial y espectral son logradas a través de la solución de problemas inversos a partir de un conjunto de mediciones codificadas de baja resolución. En este proyecto, se presentan dos modelos ópticos complementarios para super-resolución espacial y espectral (SR-CASSI). Estos modelos permiten la reconstrucción de cubos de datos hyper-espectrales super-resueltos, donde el número de bandas o planos espectrales y resolución espacial son aumentadas significativamente. Los sistemas propuestos no solo ofrecen ahorros significativos en tamaño, peso y energía, sino además en costos debido a que detectores de baja resolución pueden ser utilizados. Los resultados de las simulaciones del sistema propuesto muestran un mejoramiento de mas de 4 dB en relación señal a ruido (SNR) para el modelo de super-resolución espacial y un cubo de datos cuatro veces más resuelto espectralmente. Los resultados también muestran que el SNR de los cubos de datos reconstruidos con detectores de baja resolución realizando capturas adicionales, se acercan al SNR obtenido utilizando detectores de alta resolución.

[1] Trabajo de Grado

[2] Facultad de Ingenierías Fisicomecánicas. Escuela de Ingeniería de Sistemas e Informática. Director, Henry Arguello Fuentes.

Abstract

TITLE: SUPER-RESOLUTION ALGORITHM APPLIED TO SPECTRAL IMAGES ACQUIRED VIA COMPRESSIVE SENSING TECHNIQUE [1]

AUTHOR:HOOVER FABIÁN RUEDA CHACÓN [2]

KEYWORDS: Spectral imaging, super-resolution, compressive sensing, code-aperture based optical systems

Code-aperture based optical imaging systems are at the forefront of optical imaging modeling since they allow to capture three-dimensional scenes of spectral information in a single two-dimensional snapshot, instead of scanning the whole region line by line using spectral slit based optical instruments or similar systems. The Code Aperture Snapshot Spectral Imaging system (CASSI) is a remarkable optical imaging architecture that senses the spectral information of a scene using the underlying concepts of compressive sensing (CS). The goal of this thesis is to capture high-resolution hyper-spectral scenes in compressed signals measured by low-resolution focal plane array (FPA) detectors. Spatial and spectral super-resolution are attained through inverse problems from a set of low-resolution coded measurements. In this research project, we present two complementary optical models for spatial and spectral super-resolution imaging (SR-CASSI). These models allow the reconstruction of super-resolved hyper-spectral data cubes, where the number of spectral bands and spatial resolution are significantly increased compared with CASSI. The proposed system not only offers significant savings in size, weight and power, but also in cost, since low resolution detectors can be used. The simulation results of the proposed system show an improvement of up to 4 dB in signal to noise ratio (SNR) for spatial super-resolution and a four-fold increase in spectral resolution. Results also show that the SNR of the reconstructed data cubes approaches the SNR of the reconstructed data cubes attained with high-resolution detectors, at the cost of using additional measurements.

[1] Research Work

[2] Faculty of Physical-Mechanical Engineering. Department of Computer and Informatics Engineering. Advisor, Henry Arguello Fuentes.

Introduction

Spectrometers are a class of instruments, that measure the intensity, or polarization of electromagnetic waves across a broad range of wavelengths. Most instruments are restricted to narrow bands of the spectrum, which can include large wavelengths such as infrared and microwaves, visible light and small wavelengths as in ultraviolet, X-rays, and gamma rays [1]. Spectrometers in the visible spectrum are sometimes referred to as spectrophotometers. Spectrometers give precise wavelength information of a scene, but spatial information is restricted to the measurement location. If a scene or object has many spectral and spatial characteristics, it is necessary to scan the entire object. This is referred to as pushbroom or whiskbroom scanning [2]. For a code-aperture based spectral imager this is not necessary since the scene is encoded both spatially and spectrally using the theory of compressive sensing (CS) [3; 4; 5]. Spectrometers of this type are referred to as spectral imagers or hyper-spectral imagers. Hyper-spectral images are well suited for sparse representations as they exhibit high correlation between spectral bands [6; 7].

In code-aperture based optical system, the intensity on the detector cannot directly be correlated to spectral density as when common slit is used. Instead, the image captured at the detector must be processed using a reverse model of the system. This model includes the aperture code and some previous knowledge of the optical elements in the instrument. Code aperture snapshot spectral imager (CASSI) [8] is an imaging system that effectively exploits CS principles. It uses a single measurement to sense a complete spatio-spectral data cube. The CASSI instrument is depicted in Figure 1.

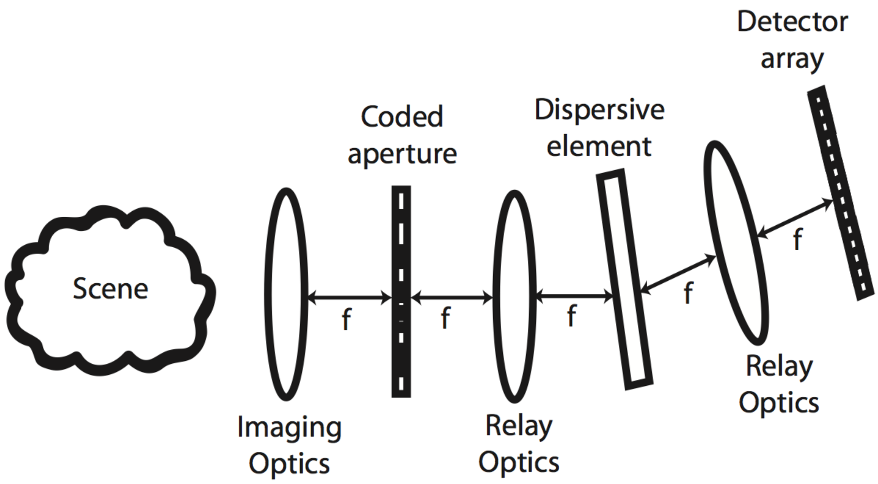

Figure 1: Code Aperture Snapshot Spectral Imaging (CASSI) optical model

CASSI is composed by an objective lens, which focuses the 3D scene, a code aperture that modulates spatially the spatio-spectral information, and a band-pass filter allowing limiting the spectral range of action. CASSI has also a dispersive element (commonly a prism), which shifts horizontally each spectral band respect to their wavelength and a focal plane array (FPA) detector, which integrates, and captures the 3D scene in a 2D array. For energy transmission between optics elements detailed above, a set of relay lenses is used. Recent studies have shown that using multiple CASSI [9] measurements instead of a single measurement provides better data cube reconstructions [10; 11; 12; 13].

High quality in data cube reconstructions depends directly on the resolution of the detector. But high-resolution detectors mean high costs. Spatial and spectral super-resolution in code aperture based optical imagery systems (SR-CASSI) are of high interest because high-resolution reconstructions can be attained from low-resolution/cost detectors. Spectral imaging in infrared (IR) wavelengths is one of the principal examples where FPAs are critical components because they become very costly with increased resolution [14]. In our previous works [15; 16], we explored spatial and spectral super-resolution in CASSI where slightly results in spatial and spectral resolution were obtained. Here, we propose and detail the mathematical model to obtain spatial and spectral super-resolution in code-aperture based optical imaging systems. Also, we deepen into the simulations and experiments, obtaining significantly improvements in both spatial and spectral data cube reconstructions.

Formally, a hyper-spectral signal $\mathbf{F} \in \mathbb{R}^{M \times N \times L}$, or its vector representation $\mathbf{f} \in \mathbb{R}^{M \cdot N \cdot L}$, is *S-sparse* on some basis $\mathbf{\Psi}$, such that $\mathbf{f} = \mathbf{\Psi}\theta$ can be approximated by a linear combination of S vectors from $\mathbf{\Psi}$ with $S \ll (N \cdot M \cdot L)$. The spectral data cube $\mathbf{F}$ has L spectral bands, and $N \times M$ pixels in spatial resolution. The theory of compressive sensing (CS) shows that $\mathbf{f}$ can be recovered from m random projections with high probability, when $m \leq S \log(N \cdot M \cdot L) \ll (N \cdot M \cdot L)$. The random projections in CASSI are represented by $\mathbf{g} = \mathbf{Hf}$ where $\mathbf{H}$ represents the transmission optical function of the system accounting for the code aperture and the dispersive element [17]. The random projections for SR-CASSI are given by $\mathbf{g} = \mathbf{DHf}$, where $\mathbf{D}$ represents the decimation transformation due to the low-resolution detector. For spatial SR-CASSI the $\mathbf{H}$ matrix represents the effect of the high-resolution code aperture $T(x, y)$ and the dispersive element. On the other side, for spectral SR-CASSI the $\mathbf{H}$ matrix represents both high-resolution code apertures $T_1(x, y)$ and $T_2(x, y)$, and the dispersive element operation.

Organization of the thesis: Code aperture snapshot spectral imaging system is presented in Section 1. The proposed methodology to obtain spatial super-resolution in code aperture-based hyper-spectral imagery systems is presented in Section 2. Thereafter, an extension for spectral super-resolution is detailed in Section 3. In Section 4, the simulations and experimental configurations are shown. Finally in Section 5, the conclusions, contributions and future work are presented.

Chapter 1

Code Aperture Snapshot Spectral Imaging (CASSI)

1.1 CASSI description

Code aperture snapshot spectral imaging (CASSI) uses combinations of code apertures and one or more dispersive elements to modulate the optical field from a scene [18]. A 2D detector array captures a single multiplexed projection of the full 3D datacube. The nature of the multiplexing performed depends on the relative position of the code aperture(s) and the dispersive element(s) within the instruments. The number of measurements is significantly smaller than the number of voxels in the datacube that are eventually reconstructed. Compressive sensing techniques, may be used to reconstruct the datacube. Due to the modulation of the datacube using a code aperture, CASSI systems do not measure certain voxels.

The CASSI instrument developed in [8] is shown in Fig. 1.1. A standard imaging lens is used to form an image of a remote scene in the plane of the code aperture. The code aperture modulates the spatial information over all wavelengths in the datacube with the coded pattern. Imaging the datacube from this plane through the dispersive element results in multiple images of the code-modulated scene at wavelength-dependent locations on the detector

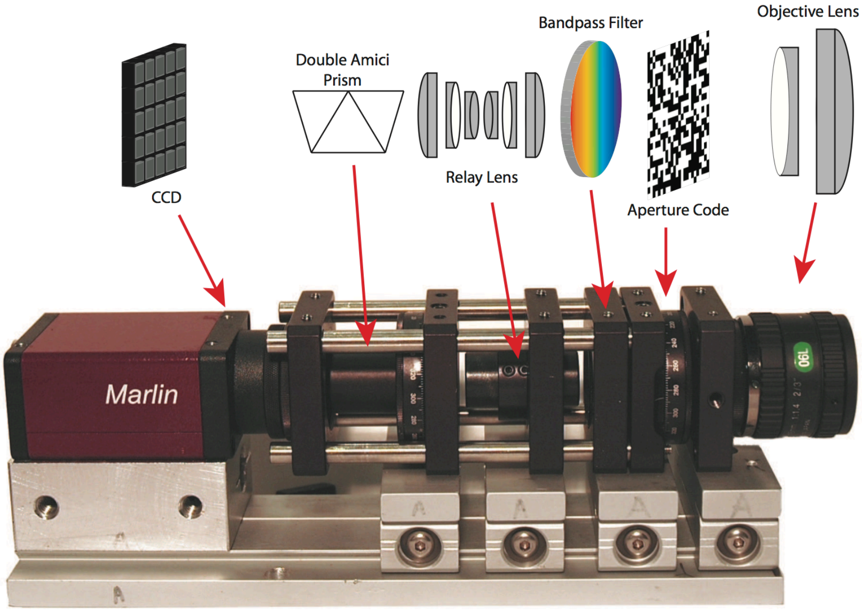

Figure 1.1: Code Aperture Snapshot Spectral Imager architecture

array. The intensity pattern measured on the detector contains a coded mixture of spatial and spectral information about the scene.

Figure 1.2 demonstrates the three step sensing process on the datacube (spatial modulation, spectral shearing and detector integration). The instrument disperses spectral information from each spatial location in the scene over a certain area across the detector. Thus, spatial and spectral information from the scene is multiplexed on the detector pixels. In CASSI, measuring just one spectrally-dispersed projection of the datacube that is spatially modulated by the aperture code over all wavelengths can be used to estimate the entire datacube.

The spatial resolution of the reconstructed datacube depends on (i) the point spread function (PSF), $h(x', x, y', y,)$, of the relay optics and dispersive element, (ii) the pixel size, Δ, (iii) the size of a feature on the code aperture, and (iv) numerical estimation effects. However, ignoring numerical estimation effects, the spatial resolution is approximately given by the width and height of the smallest feature on the code aperture. The spectral resolution of the

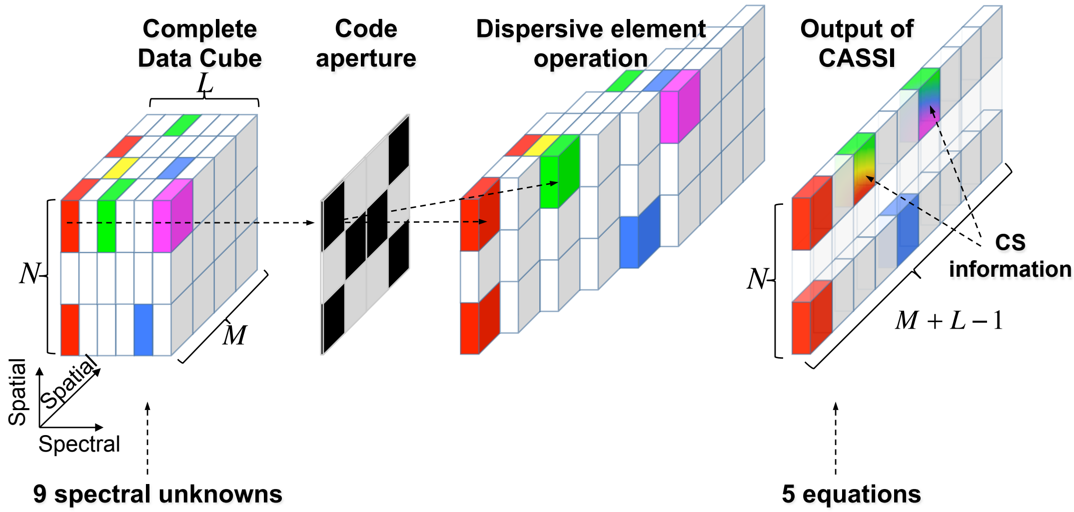

Figure 1.2: CASSI light propagation

reconstructed datacube is the separation between spectral channels in the reconstructed datacube (in nanometres). The spectral resolution of the reconstructed datacube depends on (i) the amount of dispersion induced by the dispersive element, (ii) the PSF, (iii) the pixel size, and (iv) the size of the smallest feature on the code aperture

1.2 CASSI system model

Here it is presented the model that describes the propagation of light through the instrument. The power spectral density of the image of the scene formed by the objective lens at the plane of the aperture code is denoted as $f_0(x, y, \lambda)$. Denoting the code aperture transmission function by $T(x, y)$, the power spectral density immediately after spatially modulated by the code aperture is,

$$f_1(x, y, \lambda) = T(x, y) f_0(x, y, \lambda). \tag{1.1}$$

The pattern printed in $T(x, y)$ is designed as an array of square features (pixels) with size similar to the detector pixels Δ. Let $t_{i,j}$ represent the binary value at the $(i, j)^{th}$ element, with a 1 representing a transmissive code element and a 0

representing a obstructing code element. Then, $T(x, y)$ can be described as,

$$T(x,y) = \sum_{i,j} t_{i,j} \tau(i,j;x,y), \tag{1.2}$$

where $\tau(i, j; x, y)$ represents the pixel function,

$$\tau(i,j;x,y) = \text{rect}\left(\frac{x}{\Delta} - i, \frac{y}{\Delta} - j\right). \tag{1.3}$$

After propagation through relay optic lens and the dispersive element, the power spectral density in front of the FPA detector is given by,

$$f_2(x,y,\lambda) = \iint f_1(x,y,\lambda) h(x' - S(\lambda) - x, y' - y) dx' dy' \tag{1.4}$$

where $h(x' - S(\lambda) - x, y' - y)$ represents the relay lenses and dispersive element operation and $S(\lambda)$ the dispersion induced by the dispersive element. Finally, the FPA detector measures the intensity of incident light rather than the spectral density as in spectrometers. This is done by integrating the power spectral density along the wavelength axis over the FPA spectral range Λ. Then, the measurement at the FPA is given by,

$$g(x,y) = \int_{\Lambda} f_2(x,y,\lambda) d\lambda. \tag{1.5}$$

Replacing Eq. (1.4) in Eq. (1.5) conduces to,

$$g(x,y) = \int_{\Lambda} \iint T(x',y') f_0(x',y',\lambda) h(x' - S(\lambda) - x, y' - y) dx' dy' d\lambda. \tag{1.6}$$

Assuming, (i) the PSF $h(x' - x, y' - y)$ is shift invariant, (ii) the dispersion by the dispersive element is linear, and (iii) that there is one-to-one mapping between elements of the aperture code to the detector pixels, the FPA measurement can be succinctly expressed as,

$$g(x,y) = \int_{\Lambda} T(x - S(\lambda), y) f_0(x - S(\lambda), y, \lambda) d\lambda. \tag{1.7}$$

These assumptions permit to interpret the CASSI measurement as a linear process. Experimentally, however, the PSF varies across the field, the dispersion is non-linear over CASSI's spectral range, and there are sub-pixel misalignments between the aperture code features and detector pixels. In discrete form, the measurement at the $(m,n)^{th}$ FPA pixel is given by,

$$g_{m,n} = \sum_{k=1}^{L} t_{i-k,j} f_{i-k,j,k} \tag{1.8}$$

with L being the number of datacube hyperspectral bands. In matrix form, (1.8) can be expressed as,

$$\mathbf{g} = \mathbf{H}\mathbf{f}, \tag{1.9}$$

where $\mathbf{H}$ matrix represents the CASSI sensing process accounting for CASSI optical elements operation on the discretized datacube.

Assuming a $N \times M \times L$ datacube as in Fig. 1.2, a prism exhibiting linear dispersion, shift horizontally each spectral band along x-axis by one pixel each, causing the power spectral density impinges into $N(M+L-1)$ FPA pixels. Then, CASSI sensing matrix $\mathbf{H}$ is of size $N(M+L-1) \times NML$. Hence, a datacube reconstruction $\tilde{\mathbf{f}}$ in CASSI relies on the solution of an under-determined ill-posed equations system.

1.3 CASSI reconstruction process

CASSI datacube reconstructions uses the measurement $\mathbf{g}$ and an estimation of $\mathbf{H}$ matrix. As the number of pixels on the detector used for the measurement is smaller than the number of voxels in the discrete datacube, the equations system depicted in Eq. (1.9) is under-determined. If linear inversion is attempted, this problem has an infinite number of solutions since the associated null space is non-trivial.

The signal processing theory proposes several ways to recover compressed signals. A relatively new field of study called compressive sensing (CS), gives a widely set of solutions where sensing under Shannon-Nyquist theorem is performed [3; 4]. The CS theory suggests that an under-determined problem is well-posed for inversion if the signal of interest (the datacube) is sparse or compressible in some orthonormal basis, $\mathbf{\Psi}$ and, the measurement system (CASSI) is designed so that the linear projection implemented by the sensing matrix ($\mathbf{H}$), does not significantly damage the information in any sparse or compressible signal through the dimensionality reduction [5]. Hence, the datacube is represented by,

$$\mathbf{f} = \mathbf{\Psi}\theta, \tag{1.10}$$

where θ are the sparse coefficients representation of the datacube on the basis $\mathbf{\Psi}$. Then, the compressive FPA measurements are given by,

$$\mathbf{g} = \mathbf{H}\mathbf{\Psi}\theta. \tag{1.11}$$

In this way, a hyper-spectral image datacube reconstruction $\tilde{\mathbf{f}}$ for CASSI can be achieved by solving the optimization problem,

$$\tilde{\mathbf{f}} = \mathbf{\Psi}\{\mathrm{argmin}_{\theta'}\|\mathbf{f} - \mathbf{H}\mathbf{\Psi}\theta'\|_2^2 + \tau\|\theta'\|_1\} \tag{1.12}$$

where $\tau > 0$ is a regularization parameter that balances the conflicting tasks of minimizing the least square of the residuals, while at the same time, yielding a sparse solution.

Chapter 2

Spatial Super-Resolution in CASSI

The principal objective in spatial hyper-spectral super-resolution is to obtain a high-resolution reconstruction from a set of measurements captured with low-resolution FPAs. Figure 2.1 shows the optical architecture proposed for spatial SR-CASSI to achieve this objective. In there, the image source density denoted as $f_0(x, y, \lambda)$ is first coded by the high-resolution code aperture $T(x, y)$. The resulting coded field $f_1(x, y, \lambda)$ is subsequently shifted horizontally by a dispersive element before it impinges onto the FPA, resulting in the signal $f_2(x, y, \lambda)$. The output $f_2(x, y, \lambda)$ is then optically relayed into the FPA, where the compressive measurements are realized by the integration over the detector's spectral range sensitivity.

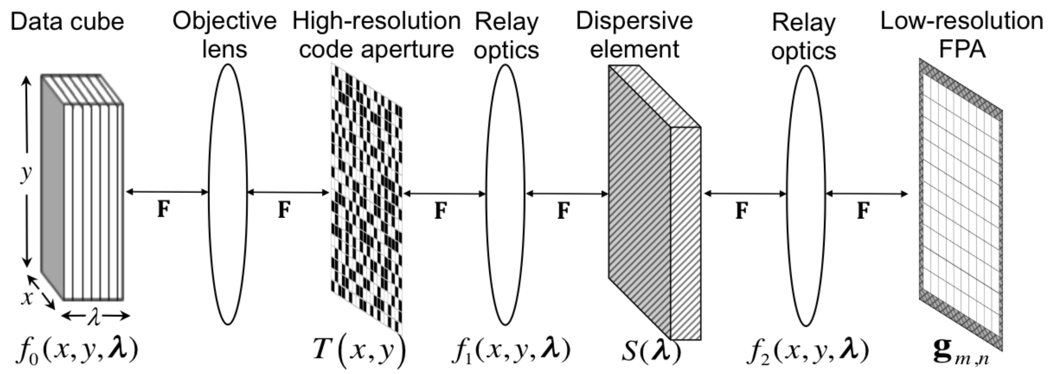

Figure 2.1: Spatial Super-resolution optical model. The FPA pixel pitch is greater than the one from the code aperture, there is not 1:1 matching between pixels.

2.1 Spatial SR-CASSI mathematical model

Assuming a $N \times M \times L$ data cube as depicted in Fig. 2.2, with $N \times M$ representing the spatial dimensions and L the spectral depth, the spatial SR-CASSI model is represented as follows. The spatial modulation realized by the code aperture can be written as,

$$f_1(x, y, \lambda) = T(x, y) f_0(x, y, \lambda). \tag{2.1}$$

The modulated spatio-spectral information is then shifted horizontally by the dispersive element. The signal obtained after dispersion is denoted as,

$$f_2(x, y, \lambda) = \iint f_1(x, y, \lambda) h(x' - x - S(\lambda), y' - y) dx' dy' \tag{2.2}$$

where $h(x' - x - S(\lambda), y' - y)$ represents the dispersive element operation with $S(\lambda)$ representing the dispersion function which depends on the spectral band wavelength. The compressive sensing measurements across the FPA are realized by the integration of the field $f_2(x, y, \lambda)$ over the detector's spectral range sensitivity,

$$g(x, y) = \int_{\Lambda} f_2(x, y, \lambda) d\lambda. \tag{2.3}$$

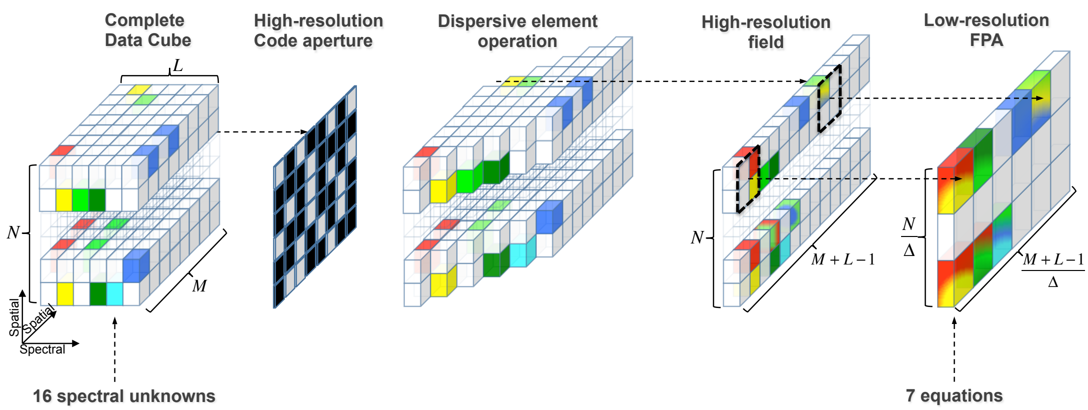

Figure 2.2: Spatial SR-CASSI sensing model

Assuming linear optical elements, we can express the analogous spatial SR-CASSI measurement as,

$$g(x,y) = \iiint T(x - S(\lambda), y) f_0(x - S(\lambda), y, \lambda) dx dy d\lambda. \tag{2.4}$$

Since the detector is spatially pixelated, the measurement at the $(m,n)^{th}$ pixel is given by,

$$g_{m,n} = \iint p(m,n;x,y) g(x,y) dx dy + \omega_{m,n}, \tag{2.5}$$

where $\omega_{m,n}$ represents additive noise and $p(m,n;x,y)$ the detector pixelation, which is given by,

$$p(m,n;x,y) = \text{rect}\left(\frac{x}{\Delta} - m, \frac{y}{\Delta} - n\right), \tag{2.6}$$

with Δ being the pixel pitch ratio between the code aperture and the detector. Then, we can express the $(m,n)^{th}$ measurement as,

$$g_{m,n} = \int_{n\Delta}^{(n+1)\Delta} \int_{m\Delta}^{(m+1)\Delta} \int_{\Lambda} T(x - S(\lambda), y) f_0(x - S(\lambda), y, \lambda) d\lambda dx dy + \omega_{m,n}. \tag{2.7}$$

A critical requirement for achieving super-resolution is that the pitch of the modulating code aperture must be lower than that of the detector. Letting Δ_c be the spatial pitch between elements in the code aperture, and Δ_d the one between detector pixels, then the pitch ratio between the code aperture and the detector is defined as $\Delta = \frac{\Delta_d}{\Delta_c}$. Assuming that the side length of the detector spans an integer number of code aperture elements, the horizontal and vertical spatial super-resolution are thus limited by Δ_c. Denoting the hyper-spectral data cube in discrete form as $(\mathbf{F}_k)_{mn}$, and the code aperture as $\mathbf{T}$, the compressive sensing measurement at the $(m,n)^{th}$ detector pixel can be written in discrete form as,

$$\mathbf{g}_{m,n} = \sum_{\ell=n\Delta+1}^{(n+1)\Delta} \sum_{j=m\Delta+1}^{(m+1)\Delta} \sum_{k=1}^{L} (\mathbf{F}_k)_{j+k,\ell} (\mathbf{T})_{j+k,\ell} + \omega_{m,n}, \tag{2.8}$$

for $m = 1, \ldots, M'$ and $n = 1, \ldots, N'$, with $M' \times N'$ being the FPA detector size.

2.2 Matrix computational approach

In matrix notation, a spatial SR-CASSI measurement is represented by,

$$\mathbf{g} = \mathbf{D}\mathbf{H}\mathbf{f}, \tag{2.9}$$

where $\mathbf{f}$ is the data cube in lexicographical notation, $\mathbf{H}$ is a $N(M+L-1)\times NML$ matrix representing the transmission function of the system accounting for the high-resolution code aperture, the dispersive element and the relay lenses. The $\mathbf{D}$ matrix is a $\frac{N(M+L-1)}{\Delta^2} \times N(M+L-1)$ matrix which represents the decimation transformation due to the low-resolution FPA. Note, that $\mathbf{f}$ represents the high-resolution hyper-spectral data cube, whereas the vector $\mathbf{g}$ the low-resolution measurement.

Multi-shot approach allows to obtain different information from the same scene as different code patterns can be used. If they are highly decoupled or independent among themselves, the full datacube voxels information can be achieved. For a multi-shot spatial SR-CASSI model, the general system can be written as,

$$\begin{bmatrix} \mathbf{g}^1 \\ \mathbf{g}^2 \\ \vdots \\ \mathbf{g}^K \end{bmatrix} = \mathbf{D} \begin{bmatrix} \mathbf{H}^1 \\ \mathbf{H}^2 \\ \vdots \\ \mathbf{H}^K \end{bmatrix} \mathbf{f}, \tag{2.10}$$

$$\tilde{\mathbf{g}} = \mathbf{D}\tilde{\mathbf{H}}\mathbf{f}, \tag{2.11}$$

where $\tilde{\mathbf{H}} \in \{0,1\}^{N(M+L-1)K\times NML}$. Notice that for multi-shot approach the code aperture pattern changes each shot. Multi-shot approach is depicted in Figure 2.3. The optical transmission function of the system for each shot can be expressed in matrix form as,

$$\mathbf{H}^i = \mathfrak{P}\mathfrak{T}^i \tag{2.12}$$

where $\mathfrak{P}$ is a $N(M+L-1)\times NML$ matrix representing the dispersive element operation and $\mathbf{T}^i$ a $NML \times NML$ block-diagonal matrix accounting for the i^{th}

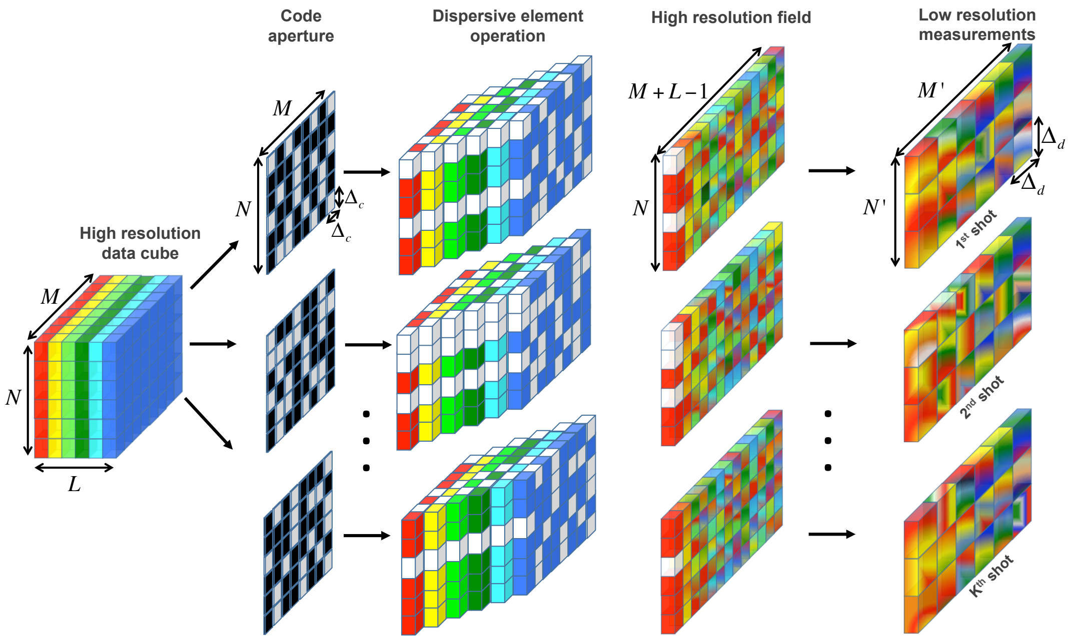

Figure 2.3: Multi-shot spatial SR-CASSI sensing model

code aperture of the form,

$$\mathfrak{T}^i = \begin{bmatrix} \text{diag}(\mathbf{t}^i) & \mathbf{0}_{NM\times NM} & \cdots & \mathbf{0}_{NM\times NM} \\ \mathbf{0}_{NM\times NM} & \text{diag}(\mathbf{t}^i) & \cdots & \mathbf{0}_{NM\times NM} \\ \vdots & \vdots & \ddots & \vdots \\ \mathbf{0}_{NM\times NM} & \mathbf{0}_{NM\times NM} & \cdots & \text{diag}(\mathbf{t}^i) \end{bmatrix}, \tag{2.13}$$

where $\mathbf{t}^i$ represents the i^{th} code aperture in lexicographical notation with size $NM \times 1$ and diag$(\cdot)$ a function which puts the elements in the argument in the diagonal of a matrix. Note that $\mathbf{0}_{NM\times NM}$ is zero-valued matrix with NM rows and columns. In the same way, the dispersive element operation is given by,

$$\mathfrak{P} = \begin{bmatrix} \text{diag}(\mathbf{1}_{NM\times 1}) & \mathbf{0}_{N\times NM} & \cdots & \mathbf{0}_{N\times NM} \\ \mathbf{0}_{N\times NM} & \text{diag}(\mathbf{1}_{NM\times 1}) & \cdots & \mathbf{0}_{N\times NM} \\ \vdots & \vdots & \ddots & \vdots \\ \mathbf{0}_{N\times NM} & \mathbf{0}_{N\times NM} & \cdots & \text{diag}(\mathbf{1}_{NM\times 1}) \end{bmatrix}, \tag{2.14}$$

where $\mathbf{1}_{a\times b}$ is a one-valued matrix with a rows and b columns. Let define $\mathbf{d} =$

$[\mathbf{1}_{1\times\Delta}\ \mathbf{0}_{1\times N-\Delta}]$. Also, define $\tilde{\mathbf{d}} = \mu_s \otimes \mathbf{d}$, where μ_s is a Δ long one-valued vector. Then, the decimation operation due to the low-resolution detector can be modeled as,

$$\mathbf{D}=\begin{bmatrix} \tilde{\mathfrak{D}} & \mathbf{0}_{NM\times NM} & \cdots & \mathbf{0}_{NM\times NM} \\ \mathbf{0}_{NM\times NM} & \tilde{\mathfrak{D}} & \cdots & \mathbf{0}_{NM\times NM} \\ \vdots & \vdots & \ddots & \vdots \\ \mathbf{0}_{NM\times NM} & \mathbf{0}_{NM\times NM} & \cdots & \tilde{\mathfrak{D}} \end{bmatrix} \tag{2.15}$$

where $\tilde{\mathfrak{D}}$ is given by,

$$\tilde{\mathfrak{D}} = \left[\tilde{\mathbf{d}}\ \tilde{\mathbf{d}}\left(\Theta_R^T\right)^{\Delta} \cdots \tilde{\mathbf{d}}\left(\Theta_R^T\right)^{N-\Delta}\right]^T \tag{2.16}$$

with Θ_R being a $N \cdot \Delta \times N \cdot \Delta$ permutation matrix of the form,

$$\Theta_R = \begin{bmatrix} 0 & 0 & \cdots & 0 & 1 \\ 1 & 0 & \cdots & 0 & 0 \\ 0 & 1 & \cdots & 0 & 0 \\ \vdots & \vdots & \ddots & \vdots & \\ 0 & 0 & \cdots & 1 & 0 \end{bmatrix} \tag{2.17}$$

$$= \begin{bmatrix} \mathbf{0}_{1\times(N\cdot\Delta-1)} & 1_{1\times1} \\ \mathbb{I}_{(N\cdot\Delta-1)\times(N\cdot\Delta-1)} & \mathbf{0}_{(N\cdot\Delta-1)\times1} \end{bmatrix} \tag{2.18}$$

where $\mathbb{I}$ is a $(N.\Delta-1)\times(N.\Delta-1)$ identity matrix. The matrix operation $\tilde{\mathbf{d}}(\Theta_R^T)^k$ shifts the columns of $\tilde{\mathbf{d}}$, k positions circularly to the right. In SR-CASSI, a set of K low-resolution FPA measurements are first captured, each having $N' \times M'$ compressed measurements, where $N' = \frac{N}{\Delta}$ and $M' = \lceil\frac{M+L-1}{\Delta}\rceil$. The number of sample measurements is often far less than the super-resolved spectral data cube voxels, hence $KN'M' \ll NML$.

2.3 Reconstruction model for spatial SR-CASSI

A hyper-spectral image datacube reconstruction $\tilde{\mathbf{f}}$ for spatial SR-CASSI can be achieved by solving the optimization problem,

$$\tilde{\mathbf{f}} = \boldsymbol{\Psi}\{\mathrm{argmin}_{\theta'} \|\mathbf{f} - \mathbf{D}\tilde{\mathbf{H}}\boldsymbol{\Psi}\theta'\|_2^2 + \tau\|\theta'\|_1\} \tag{2.19}$$

where $\tau > 0$ is a regularization parameter that balances the conflicting tasks of minimizing the least square of the residuals, while at the same time, yielding a sparse solution. A reconstruction scheme is depicted in Fig. 2.4.

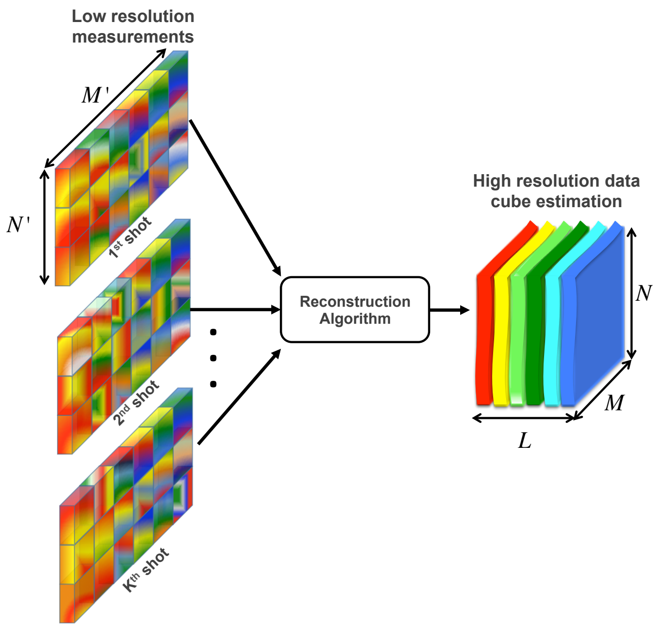

Figure 2.4: Spatial SR-CASSI data cube reconstruction

Chapter 3

Spectral Super-Resolution in CASSI

3.1 Spectral SR-CASSI model

Spectral super-resolution in code aperture multi-shot spectral imaging is attained by the system depicted in Figure 3.1, where the image source density $f_0(x, y, \lambda)$ is first coded by the code aperture $T_1(x, y)$. The resulting coded field $f_1(x, y, \lambda)$ is subsequently shifted horizontally by the dispersive element before it impinges onto the second code aperture $T_2(x, y)$. The output $f_3(x, y, \lambda)$ is then optically relayed into the FPA where the compressive measurements are realized by the integration over the detector's spectral range sensitivity.

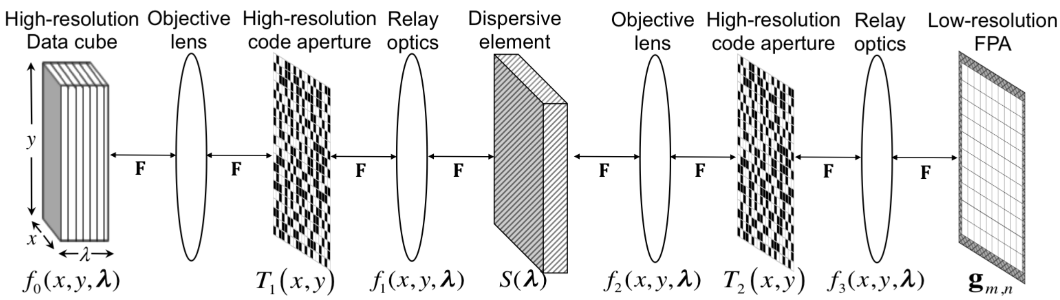

Figure 3.1: Spectral SR-CASSI architecture. The pixel pitch in both code apertures is smaller than in the FPA

The power source density impinging into the detector, after propagation through optical elements in spectral SR-CASSI, can be written as,

$$f_3(x, y, \lambda) = T_2(x, y) \iint T_1(x', y') f_0(x', y', \lambda) h(x' - x - S(\lambda), y' - y) dx' dy', \quad (3.1)$$

where $h(x' - x - S(\lambda), y' - y)$ represents the optical impulse response of the system, and $S(\lambda)$ represents the coefficient of the dispersive element. The combination of these operations, in essence, modulates the input data cube both spatially and spectrally. Furthermore, the modulation code apertures are set to have a much higher resolution than that of the detector. The source $f_0(x, y, \lambda)$ can be written in discrete form as $(\mathbf{F}_k)_{mn}$ where m and n index the spatial coordinates, and k determines the k^{th} spectral band. Then, the compressed measurements obtained at the FPA can be written in discrete form as,

$$\mathbf{g}_{m,n} = \sum_{\ell=n\Delta_d+1}^{(n+1)\Delta_d} \sum_{j=m\Delta_d+1}^{(m+1)\Delta_d} \left(\sum_{k=1}^{L} (\mathbf{F}_k)_{j+k,\ell} (\mathbf{T}_1)_{j+k,\ell} \right) (\mathbf{T}_2)_{j,\ell} + \omega_{m,n}, \quad (3.2)$$

for $n = 1, \ldots, N'$, $m = 1, \ldots, M'$, where $N' \times M'$ is the number of pixels of the FPA, Δ_d is the FPA pitch. Equation (3.2) can be rewritten in matrix notation as,

$$\mathbf{g} = \mathbf{DHf} + \omega \quad (3.3)$$

where the matrix $\mathbf{D}$ represents the decimation factor originated by the low resolution detector, $\mathbf{H}$ is the projection matrix accounting for the dispersive element and both code apertures $\mathbf{T}_1$ and $\mathbf{T}_2$ operations, and ω representing the shot noise.

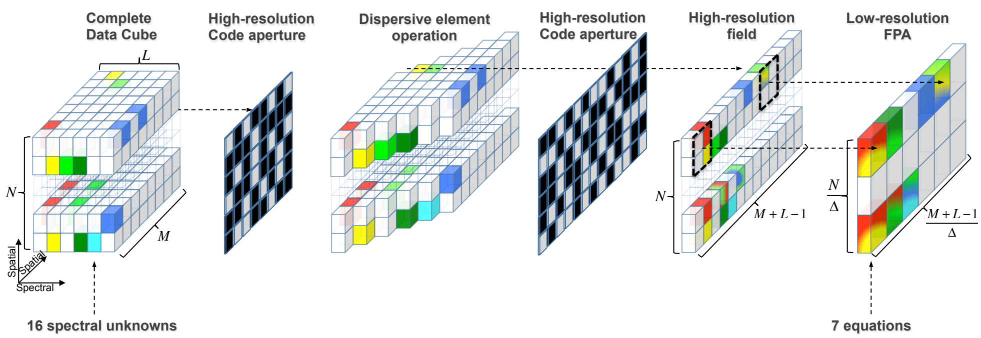

Figure 3.2: Spectral SR-CASSI sensing model

3.2 Multi-shot spectral SR-CASSI model

For a multi-shot approach, the general model for spectral SR-CASSI is similar to that for spatial SR-CASSI, and can be written as,

$$\begin{bmatrix} \mathbf{g}^1 \\ \mathbf{g}^2 \\ \vdots \\ \mathbf{g}^K \end{bmatrix} = \mathbf{D} \begin{bmatrix} \mathbf{H}^1 \\ \mathbf{H}^2 \\ \vdots \\ \mathbf{H}^K \end{bmatrix} \mathbf{f}, \tag{3.4}$$

$$\tilde{\mathbf{g}} = \mathbf{D}\tilde{\mathbf{H}}\mathbf{f}, \tag{3.5}$$

where $\tilde{\mathbf{H}} \in 0, 1^{N(M+L-1)K \times NML}$. The difference between spatial and spectral SR-CASSI lies in the optical transmission function $\tilde{\mathbf{H}}$. Notice that for multi-shot approach both code aperture patterns change every shot. Multi-shot approach for spectral SR-CASSI is depicted in Figure 3.3. The optical transmission func-

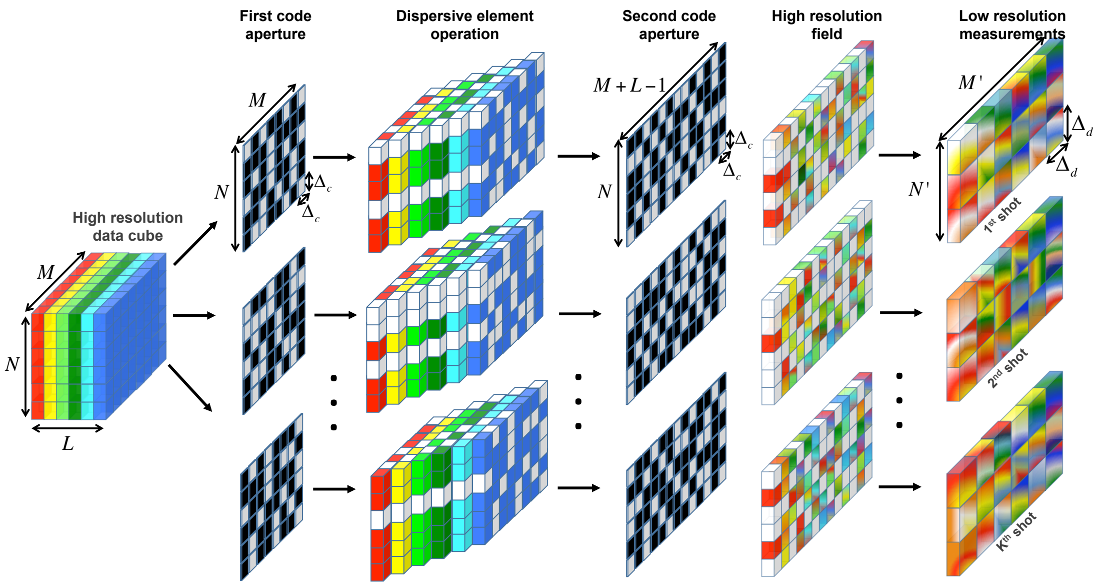

Figure 3.3: Multi-shot spectral super-resolution sensing model

tion of the system can be expressed in matrix form by,

$$\mathbf{H}^i = \mathfrak{T}_2^i \mathfrak{P} \mathfrak{T}_1^i \tag{3.6}$$

where $\mathfrak{P}$ is a $N(M+L-1) \times NML$ matrix representing the dispersive element operation, $\mathfrak{T}_1^i$ a $NML \times NML$ block-diagonal matrix accounting for the i^{th} first code aperture of the form,

$$\mathfrak{T}_1^i = \begin{bmatrix} \text{diag}(\mathbf{t}_1^i) & \mathbf{0}_{NM\times NM} & \cdots & \mathbf{0}_{NM\times NM} \\ \mathbf{0}_{NM\times NM} & \text{diag}(\mathbf{t}_1^i) & \cdots & \mathbf{0}_{NM\times NM} \\ \vdots & \vdots & \ddots & \vdots \\ \mathbf{0}_{NM\times NM} & \mathbf{0}_{NM\times NM} & \cdots & \text{diag}(\mathbf{t}_1^i) \end{bmatrix} \tag{3.7}$$

where $\mathbf{t}_1^i$ represents the i^{th} first code aperture in lexicographical notation with size $NM \times 1$. Note that $\mathbf{0}_{NM\times NM}$ is zero-valued matrix with NM rows and columns. Straightforward, the second code aperture $\mathfrak{T}_2^i$ operation is modelled in the system as a $N(M+L-1) \times N(M+L-1)$ matrix, with the values of the i^{th} second code aperture in its diagonal. Both, the dispersive element operation and the decimation due to the low-resolution FPA are modelled similarly to those in spatial SR-CASSI, given by Eqs. (2.14) and (2.15).

In spectral SR-CASSI, as in spatial SR-CASSI a set of K low-resolution FPA measurements are first captured, each one having $M' \times N'$ compressed measurements. The number of sample measurements is often far less than that of the super-resolved hyper-spectral data cube. Hence, $KN'M' \ll NML$, N' and M' are given by $N' = \frac{N}{\Delta}$ and $M' = \lceil \frac{M+L-1}{\Delta} \rceil$. Assume the distance between elements in both code apertures be Δ_c. Then, the pitch ratio between the FPA and the aperture codes can be defined as $\Delta = \frac{\Delta_d}{\Delta_c}$. Also, assuming that the band pass filter of the instrument limits the spectral components between λ_1 and λ_2, the number of super-resolvable bands L have an upper bound given by $L = \alpha\Delta\frac{\lambda_2-\lambda_1}{\Delta_d}$. The spectral super-resolution is then determined by $\frac{\alpha}{\Delta_c}$.

3.3 Reconstruction model for spectral SR-CASSI

A hyper-spectral image datacube reconstruction $\tilde{\mathrm{f}}$ for spectral SR-CASSI can be achieved similarly to spatial SR-CASSI, by solving the optimization problem,

$$\tilde{\mathbf{f}} = \mathbf{\Psi}\{\text{argmin}_{\theta'}\|\mathbf{f} - \mathbf{D}\tilde{\mathbf{H}}\mathbf{\Psi}\theta'\|_2^2 + \tau\|\theta'\|_1\} \tag{3.8}$$

where $\tau > 0$. Notice that spectral SR-CASSI sensing matrix $\tilde{\mathbf{H}}$, differs from the spatial SR-CASSI, in that, it accounts also for the second code aperture $\mathfrak{T}_2$.

Chapter 4

Simulations and Results

4.1 General assumptions

A hyper-spectral image datacube making the role of *the reality* is obtained from the scene depicted in Fig. 4.1, by illuminating the object using specific monochromatic sources along visible spectral range (450 nm - 642 nm), and by using a 256×256 FPA.

Figure 4.1: Original scene

Hence, a high-resolution data cube $\mathbf{F}$ exhibiting $L = 24$ spectral bands and 256×256 pixels in spatial domain is experimentally obtained. The $256 \times 256 \times 24$ high-resolution hyper-spectral datacube is depicted in Fig. 4.2.

Having defined the power spectral source, the next step is to find the best compression basis to represent the hyperspectral datacube. As shown in Fig.

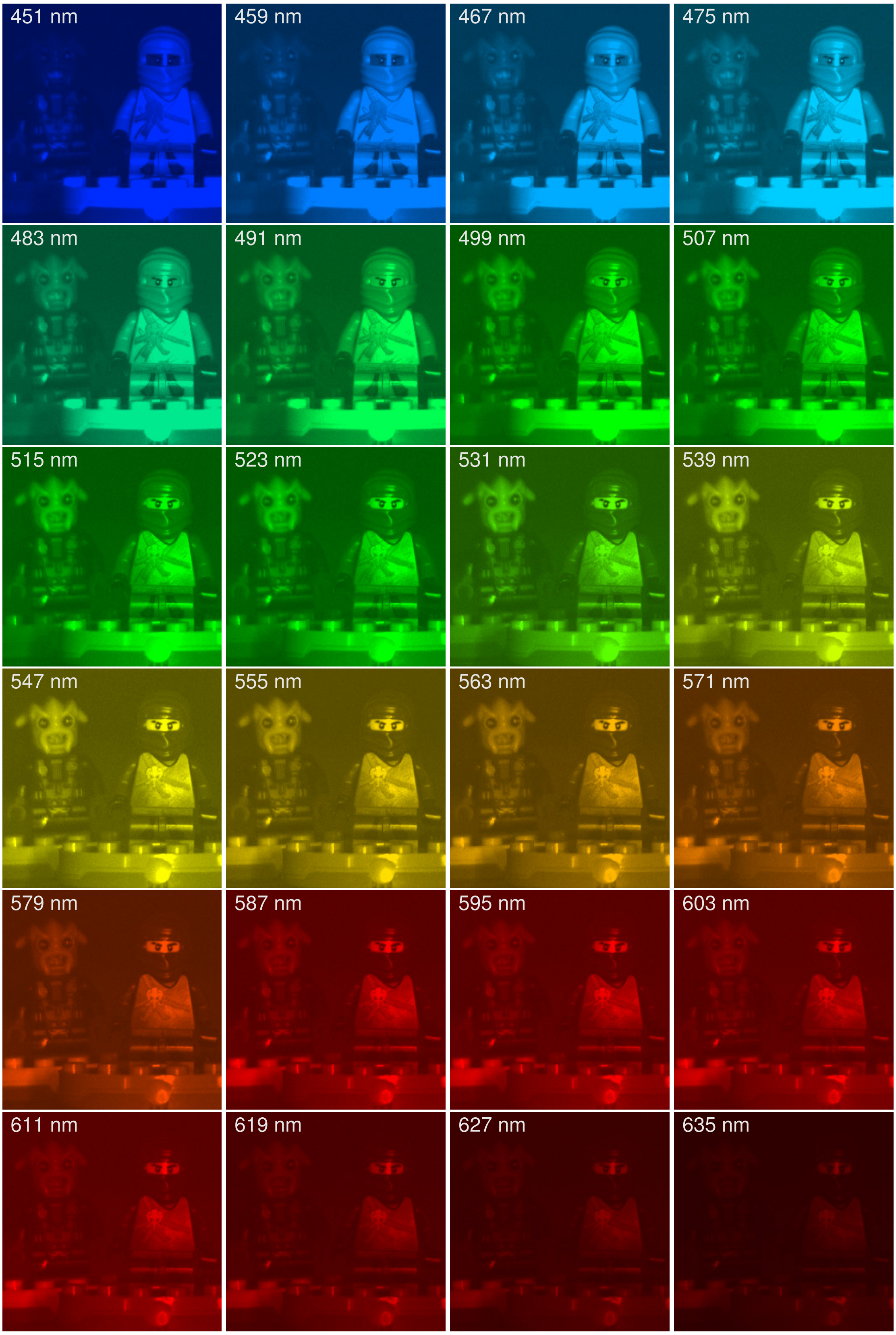

Figure 4.2: $256 \times 256 \times 24$ hyperspectral data-cube

4.3, three different basis are evaluated and their representation coefficients analyzed. The hyperspectral datacube coefficients are depicted in Fig. 4.3(a).

The first compression basis evaluated is the Wavelet 1D which is applied at each datacube pixel along the spectral domain; results are depicted in Fig. 4.3(b). A second attempt is done by using the Wavelet 2D compression basis, which is applied at each spectral datacube band; the quantity of coefficients as well as the compression result is showed in Fig. 4.3(c). Finally, a 3D representation basis is obtained by using the Kronecker matrix product [19] in order to exploit the best representation basis for both spatial and spectral domain. Hence, a Discrete Cosine Transform for spectral domain and the Wavelet 2D transform for spatial compression are used, and the compression achieved is depicted in Fig. 4.3(d).

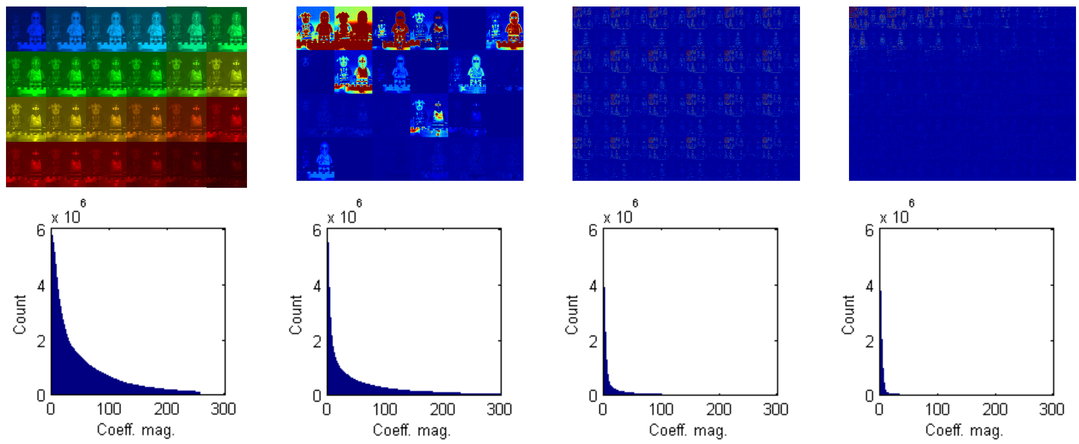

(a) Original datacube (b) Wavelet 1D basis (c) Wavelet 2D basis (d) Kronecker basis

Figure 4.3: Compression basis comparison. (a) Original scene. (b) Wavelet 1D. (c) Wavelet 2D. (d) Kronecker (DCT-Wavelet 2D)

4.2 Spatial SR-CASSI experiments performance comparison

For spatial SR-CASSI simulations, a high-resolution image cube $\mathbf{F}$ is experimentally obtained with $L = 6$ spectral bands and $N = M = 256$ pixels in spatial dimensions. In order to compare super-resolution results, we use a sub-sampled version data cube of size $64 \times 64 \times 6$. Note, the spectral range is the same for the high and low resolution data cubes, which is between $450-642nm$. The comparison method is depicted in Fig. 4.4.

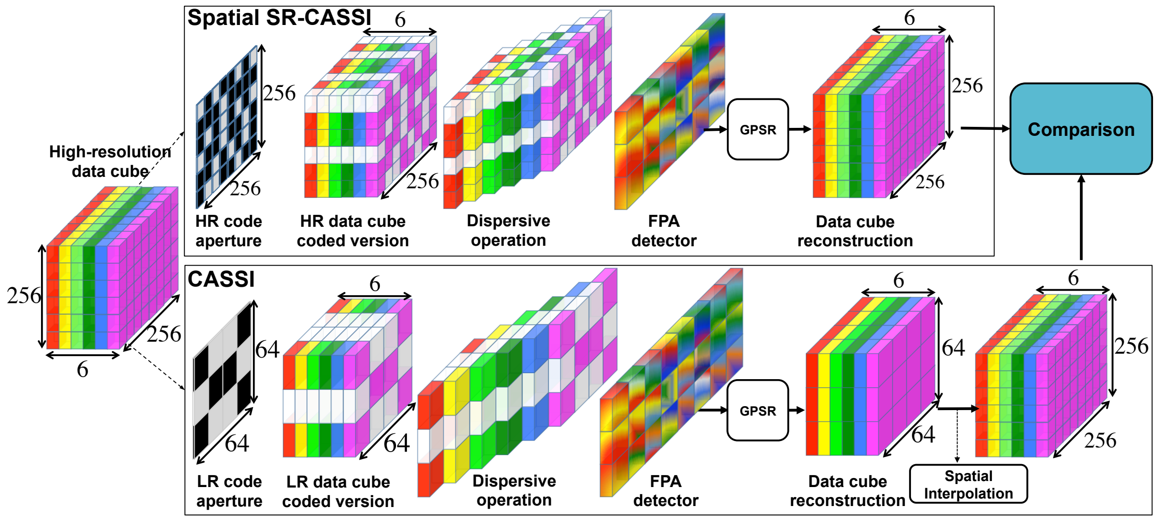

Figure 4.4: Comparison methodology for spatial SR-CASSI vs. CASSI. The SR-CASSI experiment is executed normally and a high-resolution datacube estimation is obtained. On the other side, a low-resolution datacube estimation is obtained when CASSI is used, then a spatial interpolation equivalent to the decimation factor is performed to comparison.

In our simulations, the code aperture for SR-CASSI $\mathbf{T}$ is set to the high-resolution size 256×256. The decimation ratio between the high and low resolution FPA is $16 : 1$ ($\Delta = 4$). The low-resolution FPA used in all the experiments is of size 69×64. For comparison, the CASSI code aperture was of size 64×64, exhibiting $1 : 1$ correspondence between pixels with the FPA. Figure 4.5 shows the code aperture and FPA characteristics.

The Gradient Projection for Sparse Reconstruction algorithm (GPSR) is used to reconstruct the spectral data cubes as it exhibits faster computational speed [20]. The base representation $\boldsymbol{\Psi}$ is the Kronecker product of three basis $\boldsymbol{\Psi} = \boldsymbol{\Psi}_1 \otimes \boldsymbol{\Psi}_2 \otimes \boldsymbol{\Psi}_3$, where the combination $\boldsymbol{\Psi}_1 \otimes \boldsymbol{\Psi}_2$ is the 2D-Wavelet Symlet 8 basis and $\boldsymbol{\Psi}_3$ is the Discrete Cosine basis. All the simulations were conducted and timed on the same workstation with an Intel Core 2 Duo 2.40 GHz that has 2 cores and 8 GB memory (DDR3 at 1067 MHz), running Mac OS X Snow Leopard (v. 10.6.8) and Matlab (v. 7.11.0 R2010b).

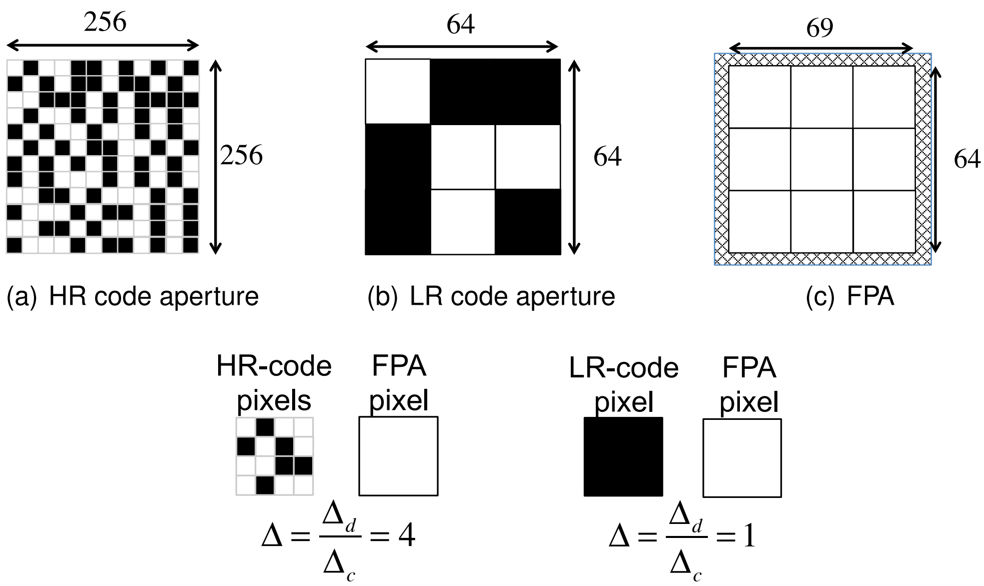

Figure 4.5: High/low-resolution code aperture and FPA characteristics. (a) High-resolution code aperture for SR-CASSI. (b) Low-resolution code aperture used in CASSI. (c) Low-resolution FPA used in both experiments. (d) Ratio between high-resolution code aperture and the FPA. (e) Ratio between low-resolution code aperture and the FPA.

Figure 4.6 shows a comparison between the super-resolution reconstruction approach described here, and the original CASSI system without super-resolution. Clearly, the super-resolution approach obtains better PSNR than the non-super-resolution case as number of shots increases. The improvement is approximately 3.5 dB better when 48 shots are measured. A 4.25 dB gain is attained with 96 shots. Notice, that CASSI does not improve as number of shots increase. This is due to the fact that no extra sub-pixel information is exploited as in the super-resolution approach.

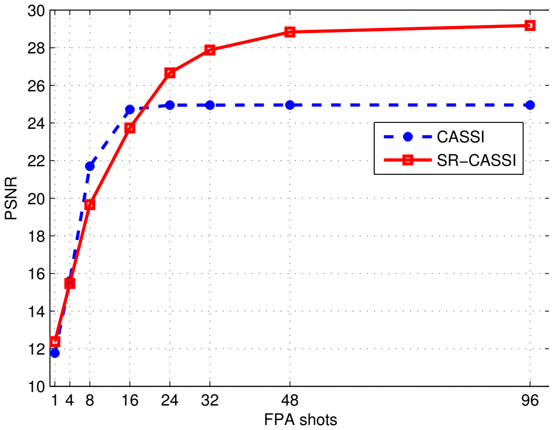

Shots	PSNR (dB)	
	CASSI	SR-CASSI
1	11.76	12.38
4	15.59	15.46
8	21.70	19.66
16	24.71	23.74
24	24.94	26.67
32	24.95	27.88
48	24.95	28.83
96	24.96	29.18

Figure 4.6: Comparison between CASSI and SR-CASSI imaging systems. The decimation in the super-resolution approach has a ratio of 4:1. SR-CASSI approach gives an approximate improvement of 4.35 dB, compared with CASSI approach that remains quasi-constant when the number of shots increases.

The six-bands datacube reconstructions results when 96 shots are captured are depicted in Fig. 4.7. Particularly, different small regions are zoomed in to see the difference between using CASSI and SR-CASSI, the results are depicted in Fig. 4.8, where the $1^{st}, 3^{rd}$ and 6^{th} spectral bands of the data cube are evaluated. In this figure, we confirm that better reconstruction results can be obtained when the super-resolution model developed is used. The PSNR remains almost constant (25 dB) indistinctly of the number of shots when the CASSI model is used. This is unlike the SR-CASSI where the PSNR increases as the number of shots grows.

Finally, the resulting reconstruction of spectral data cubes are shown in Fig. 4.9 as they would be viewed by a CCD Color Camera.

(a) CASSI datacube reconstruction at 96 shots

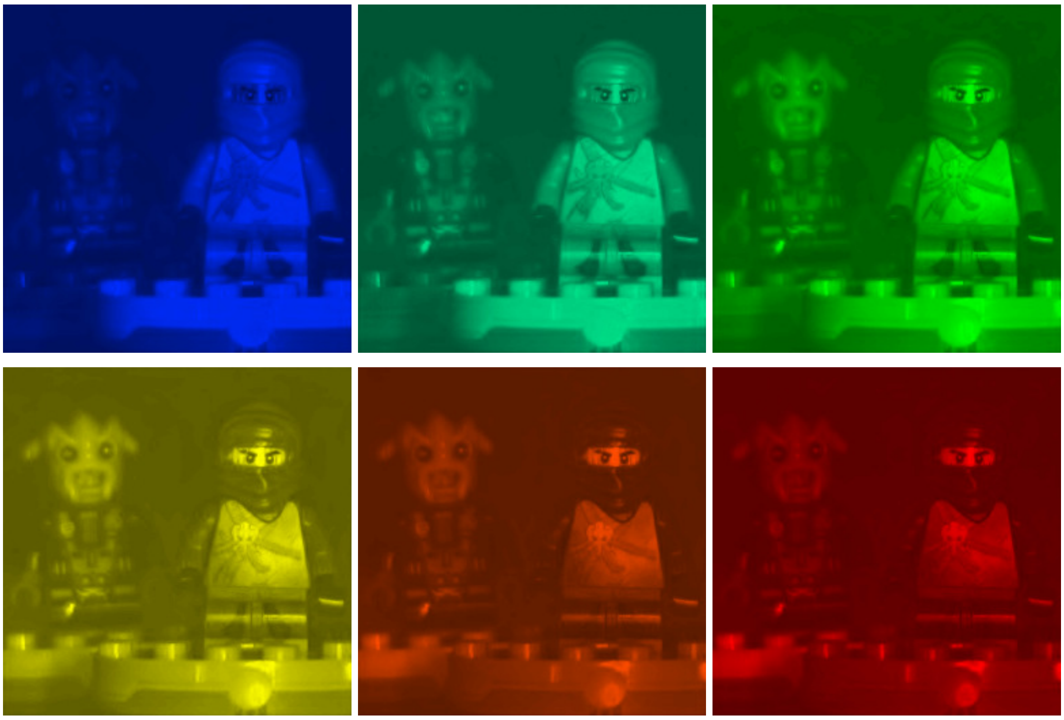

(b) Spatial SR-CASSI datacube reconstruction at 96 shots

Figure 4.7: Six-bands datacube reconstructions. (a) CASSI reconstruction result. (b) SR-CASSI datacube reconstruction when $\Delta = 4$.

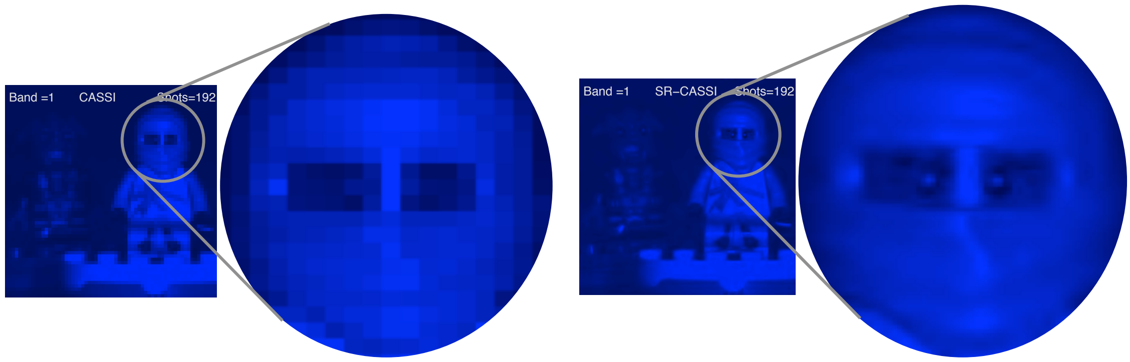

(a) 1^{st} spectral band

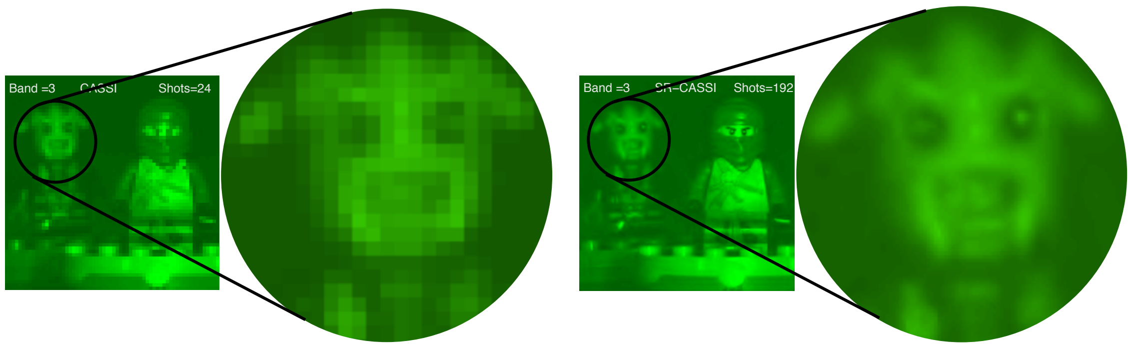

(b) 3^{rd} spectral band

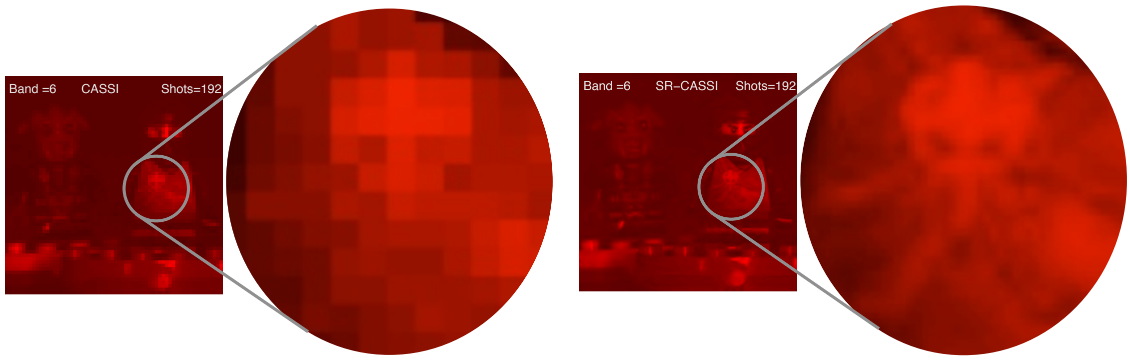

(c) 6^{th} spectral band

Figure 4.8: Visual comparison of the reconstructions of the 1^{st}, 3^{rd} and 6^{th} spectral bands from the 6 spectral band data cube. (a)-(c) CASSI vs SR-CASSI result for 1^{st}, 3^{rd} and 6^{th}, 192 shots. The averaged PSNR results were 25.04 dB for CASSI, and 29.31 dB for spatial SR-CASSI using 192 shots. SR-CASSI improves on CASSI by approximately 4.27 dB

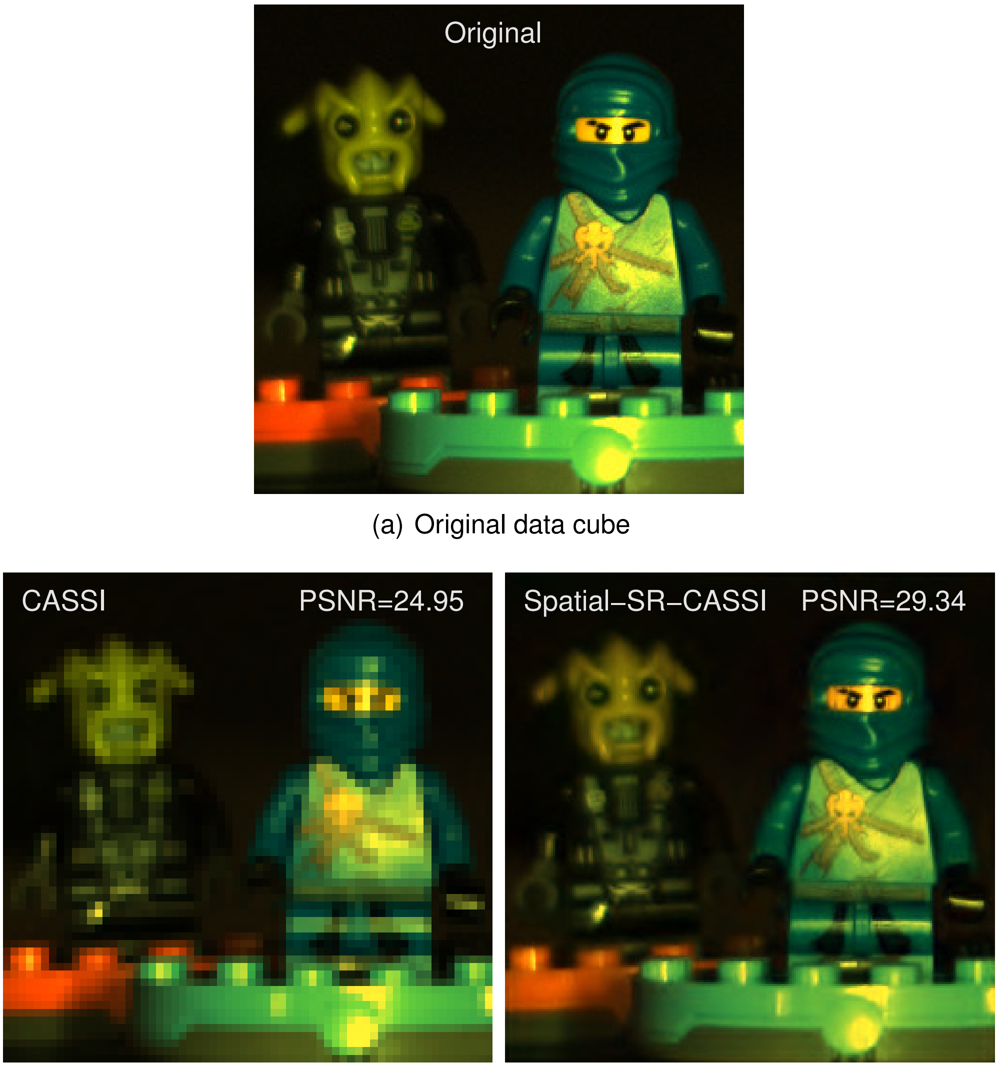

(a) Original data cube

(b) CASSI

(c) Spatial SR-CASSI

Figure 4.9: The resulting data cube reconstructions are shown as they would be viewed by a CCD Color Camera

4.3 Spectral SR-CASSI simulations

For the experiments realized in this section, a high-resolution spectrally coarse $256 \times 256 \times 6$ data-cube is used. For SR-CASSI the high-resolution code apertures, $T_1(x, y)$ and $T_2(x, y)$ exhibit spatial resolution of 256×256 and 279×256, respectively. CASSI, on the other hand uses a low-resolution code aperture matching with the pixel pitch of the low-resolution FPA. Three different low-resolution 133×128, 69×64, and 37×32 FPAs are used and compared in the experiments. That is, the decimation ratios between both high code apertures and the low resolution FPA varies between 2, 4 and 8 ($\Delta = 2, 4, 8$). Hence, CASSI code aperture resolution varies between 128×128, 64×64, and 32×32. The comparison method between both approaches is depicted in Fig. 4.10.

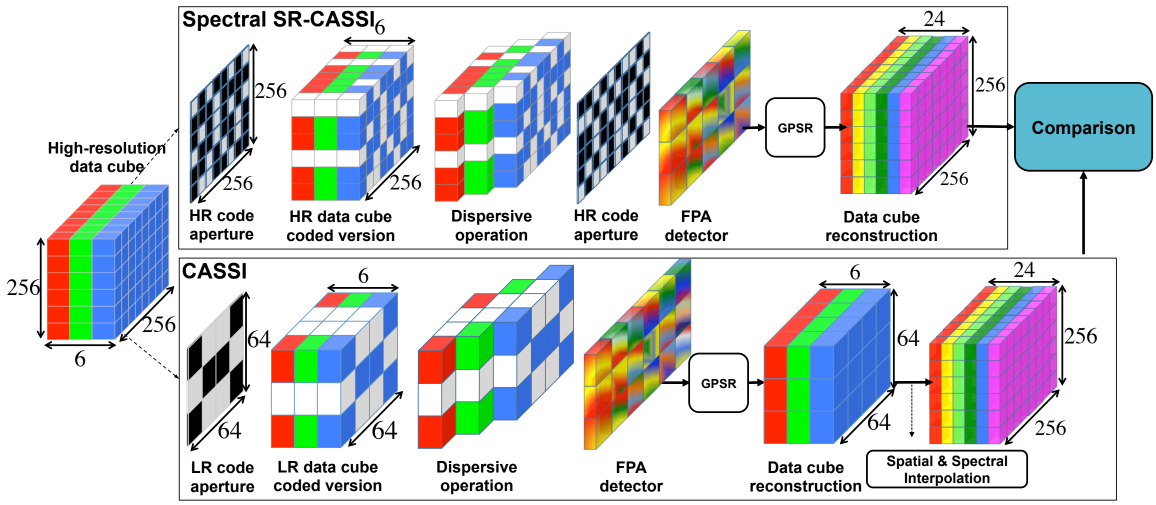

Figure 4.10: Comparison methodology for spectral SR-CASSI vs. CASSI. The SR-CASSI experiment is executed normally and a high-resolution spatially and refined spectrally datacube estimation is obtained. On the other side, a low-resolution datacube estimation is obtained when CASSI is used, then a spatial interpolation equivalent to the decimation factor is performed. Also an interpolation in the spectral domain equivalent to the ratio between the second code aperture and the FPA is realized.

Notice that, the spectral range remains the same for the high and low-resolution data cubes, which is between 451 and 642 nanometers. The bandwidth of each spectral slice in the high-resolution data cube is 8 nanometers, while the low-resolution data cube exhibits 32 nanometers per band. The representation basis $\mathbf{\Psi}$ is the Kronecker product of three basis $\mathbf{\Psi} = \mathbf{\Psi}_1 \otimes \mathbf{\Psi}_2 \otimes \mathbf{\Psi}_3$, where the combination $\mathbf{\Psi}_1 \otimes \mathbf{\Psi}_2$ is the 2D-Wavelet Symlet 8 basis and $\mathbf{\Psi}_3$ the Discrete Cosine basis. The Gradient Projection for Sparse Reconstruction algorithm (GPSR) was used to reconstruct the spectral data cubes as it exhibits faster computational speed.

For spectral SR-CASSI the density distribution of the pattern printed in the code apertures is analyzed. That is, the code apertures exhibits a binary pattern with equiprobable entries $\{0, 1\}$. A zero-valued pixel means the light propagates through this code aperture pixel, and a one-valued pixel blocks the incident light. The zero-to-ones pixel ratio in the code aperture causes the datacube reconstruction becomes harder or easier to obtain. Thereby, as more zeros a patterned code aperture exhibit, more complex the estimation becomes, due to more datacube voxels impinge onto the FPA, i.e. more unknowns appear while the number of equations remain the same. The PSNR of the reconstructed data cubes, as a function of the number of FPA measurements captured, is shown in Figs. 4.11 - 4.13, where the ratio between ones and zeros in the code apertures varies between 30% (30% ones and 70% zeros) and 50% (50% ones and 50% zeros).

Analyzing the best results, SR-CASSI obtains better PSNR than CASSI when more than 40 FPA measurements are taken for $\Delta = 2, 4$ and more than 80 for $\Delta = 8$. This improvement is approximately 8 dB, 6 dB and 2.6 dB for $\Delta = 2, 4, 8$ respectively. The CASSI PSNR remains static as number of shots increase, due to the fact that no sub-pixel information can be exploited, unlike SR-CASSI which exploits sub-pixel information by using the high-resolution code apertures. Datacube reconstructions by using CASSI and spectral SR-CASSI are depicted in 4.14. In Fig. 4.15 the zoomed version of the $1^{st}, 5^{th}, 9^{th}, 13^{th}, 17^{th}$ and 24^{th} spectral bands of the data cube are shown, in order to notice the visual improvement. The resulting reconstruction of spectral data cubes are shown in Fig. 4.16 as they would be viewed by a CCD Color Camera.

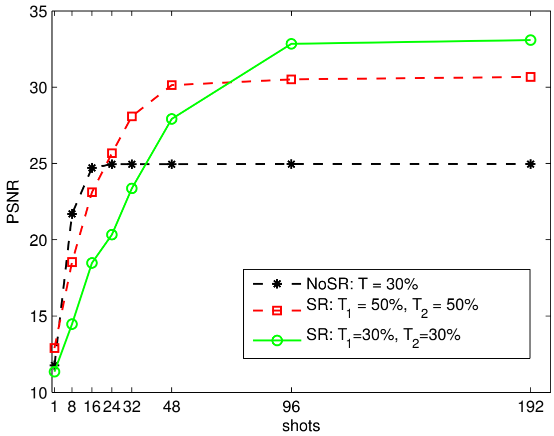

Shots	PSNR (dB)	
	CASSI	SR-CASSI
1	11.76	11.36
8	21.70	14.47
16	24.72	18.48
24	24.94	20.33
32	24.95	23.37
48	24.95	27.92
96	24.96	32.84
192	24.96	33.09

Figure 4.11: Spectral SR result for $\Delta = 2$

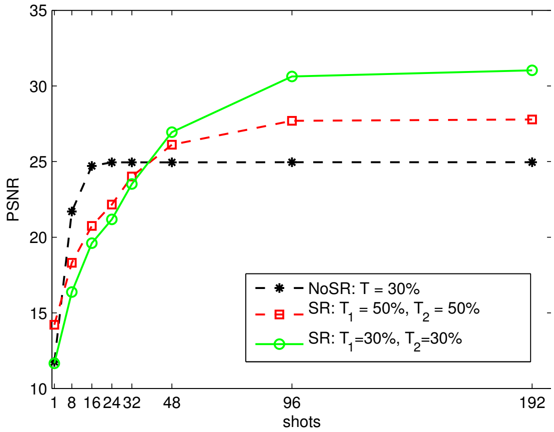

Shots	PSNR (dB)	
	CASSI	SR-CASSI
1	11.76	11.66
8	21.70	16.37
16	24.72	19.61
24	24.94	21.18
32	24.95	23.52
48	24.95	26.95
96	24.96	30.63
192	24.96	31.03

Figure 4.12: Spectral SR result for $\Delta = 4$

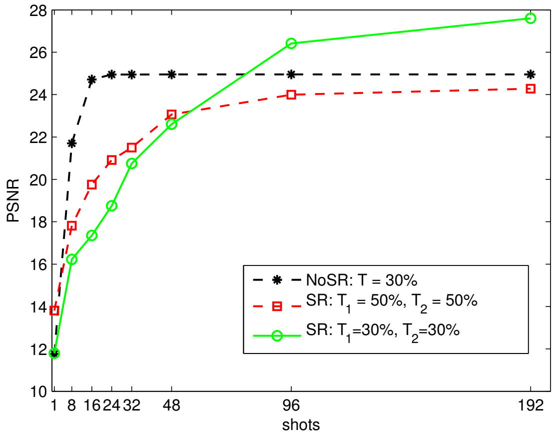

Shots	PSNR (dB)	
	CASSI	SR-CASSI
1	11.76	11.79
8	21.70	16.22
16	24.72	17.35
24	24.94	18.75
32	24.95	20.75
48	24.95	22.60
96	24.96	26.42
192	24.96	27.60

Figure 4.13: Spectral SR result for $\Delta = 8$

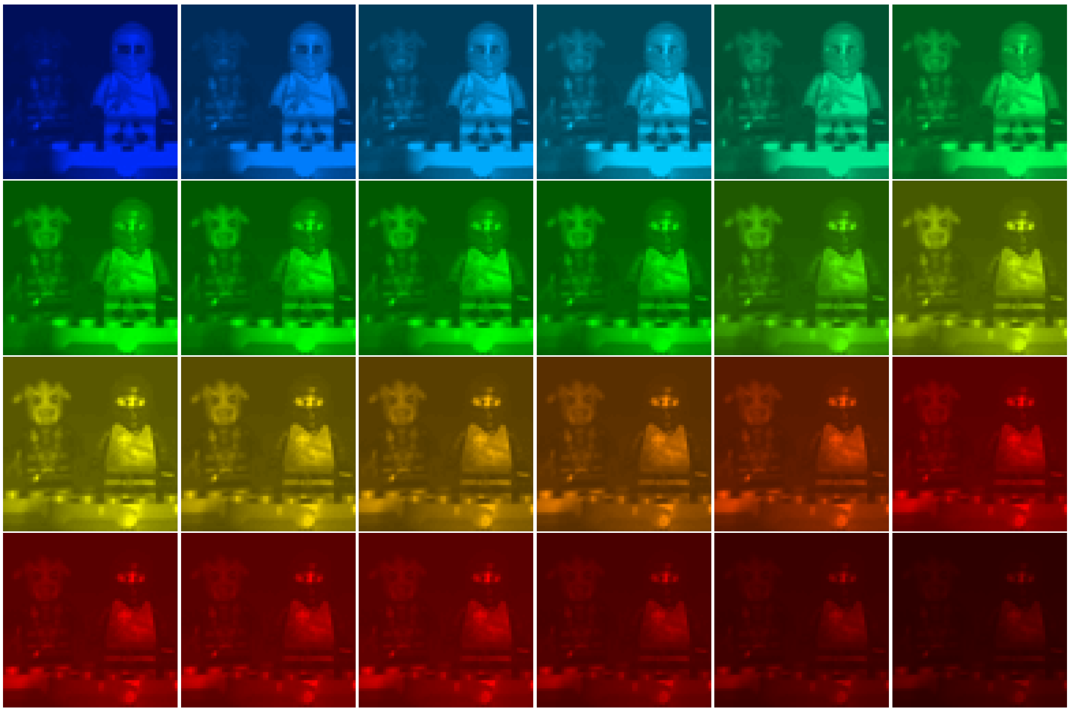

(a) CASSI datacube reconstruction at 192 shots

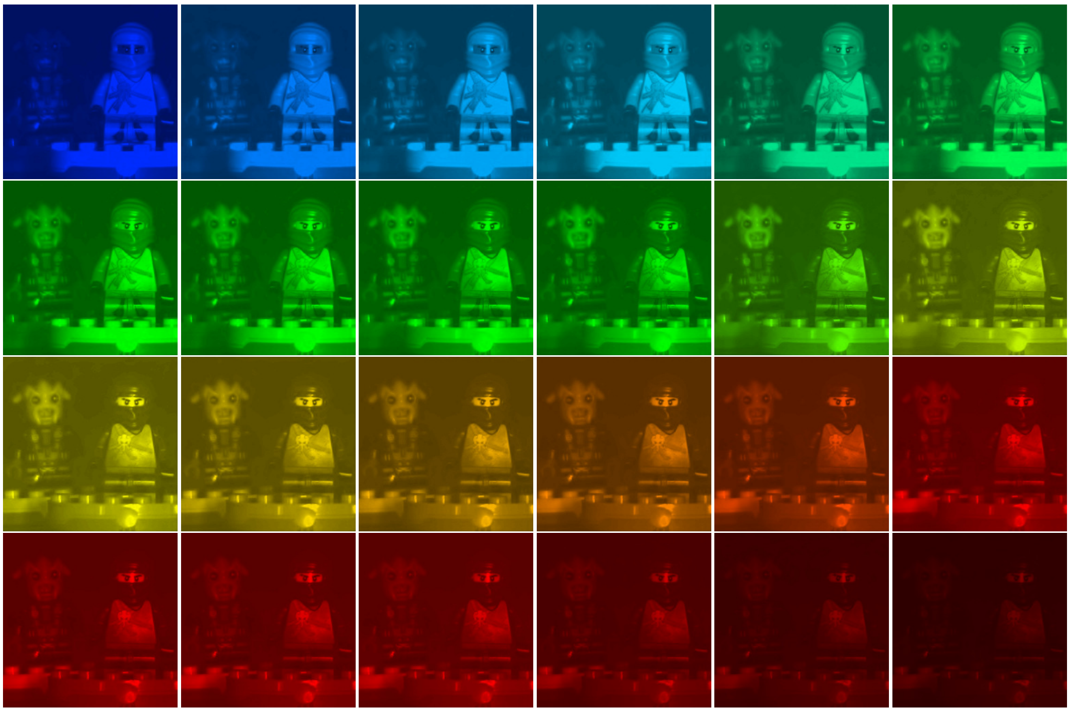

(b) Spatial SR-CASSI datacube reconstruction at 192 shots

Figure 4.14: 24-bands datacube reconstructions. (a) CASSI reconstruction spatio/spectral interpolation result. (b) SR-CASSI datacube reconstruction when $\Delta = 2$.

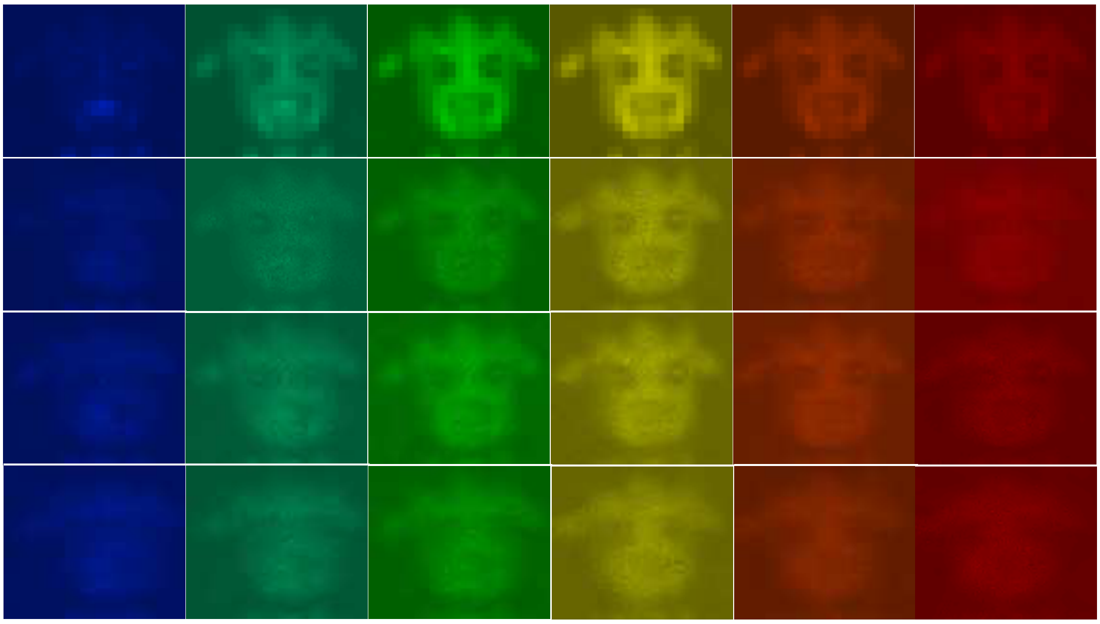

(a) Measuring 16 shots

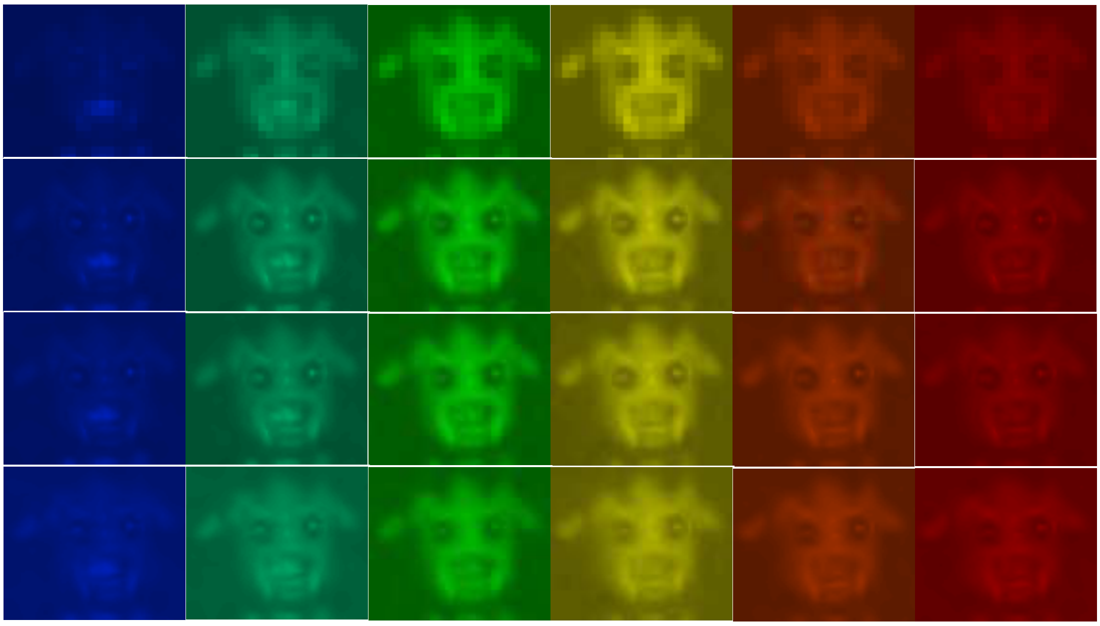

(b) Measuring 192 shots

Figure 4.15: Reconstruction of zoomed portions from $1^{st}, 5^{th}, 9^{th}, 13^{th}, 17^{th}$ and 24^{th} hyper-spectral bands. First row shows the results for CASSI. Second, third and fourth rows show the results for spectral SR-CASSI for decimation factors 2, 4 and 8 respectively. (a) For 16 FPA measurements. (b) For 192 FPA measurements.

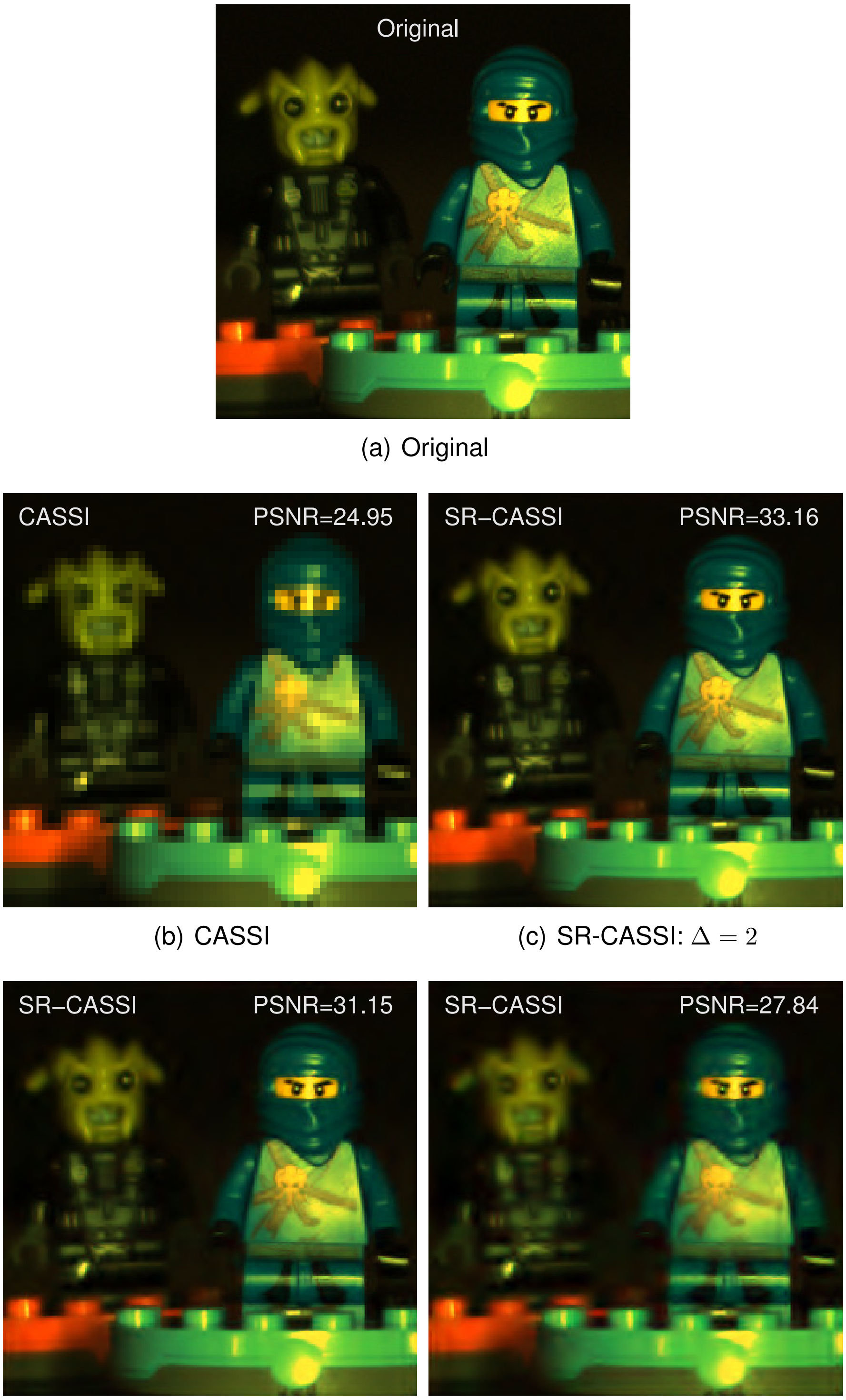

(a) Original

(b) CASSI

(c) SR-CASSI: $\Delta = 2$

(d) SR-CASSI: $\Delta = 4$

(e) SR-CASSI: $\Delta = 8$

Figure 4.16: The resulting data cube reconstructions are shown as they would be viewed by a CCD Color Camera

Chapter 5

Conclusions

- A super-resolved methodology for code-aperture based multi-shot spectral imaging systems in the visible spectral range was developed. The proposed methodology and optical architectures provide a way to effectively obtain more information from the original hyper-spectral signal by taking multiple shots where sub-pixel information can be exploited.

- Inversion of the snapshot or multishot projection for recovery of the data cube is an ill-posed problem because the number of measurements (equations) available is significantly smaller than the number of voxels (unknowns) in the datacube. Thus, the Gradient Projection for Sparse Representation method was used to numerically estimate the datacube by assuming hyperspectral signal sparsity of the scene in a Kronecker representation basis, combining the discrete cosine transform and the 2D wavelet transform.

- For spatial SR-CASSI, the simulation results show an improvement of up to 4.27 dB when the proposed methodology is used. It also represents significant savings in cost as low resolution detectors can be used instead of costly high-resolution FPAs.

- For spectral SR-CASSI, improvements of 8 dB, 6 dB and 2.6 dB in PSNR were achieved for pixel pitch ratios of 2, 4 and 8, respectively. Also, a four-fold improvement in spectral resolution was attained where a 24 spectral datacube could be reconstructed, rather than the 6-band cube made possible by the CASSI architecture.

- Multi-shot approaches improve single-shot code aperture based optical systems at the cost of take multiple FPA measurements. This approach requires that the objective remains static while multiple shots are being captured.

Contributions

- H. Arguello, H. Rueda, and G. R. Arce. ”Spatial super-resolution in code aperture spectral imaging”. *SPIE Conference on Defense, Security and Sensing*, Baltimore, MD, April 2012.
- H. Arguello, H. Rueda, and G. R. Arce. ”On super-resolved coded aperture spectral imaging”. *Submitted to IEEE Workshop on Signal Processing Systems*, Quebec, Canada, April 2012.
- H. Rueda and H. Arguello. ”Super-resolution algorithm applied to spectral images acquired by Compressive Sensing”. *In preparation to be submitted to Journal of Engineering and Research*, Universidad Nacional de Colombia, June 2012.

Future work

- H. Arguello, H. Rueda, and G. R. Arce. “Hyperspectral Super-resolution in coded aperture based optical imagery systems”. *In preparation to be submitted to IEEE Transactions on Image Processing*, 2012.
- H. Arguello, H. Rueda, Y. Wu, D. Prather and G. R. Arce. “High-Order Precision Models for Coded Aperture Spectral Imaging”. *In preparation to be submitted to Optics Express*, 2012.

Bibliography

[1] D. Kittle and D. J. Brady. Compressive spectral imaging. Master's thesis, Department of Electrical and Computer Engineering, Duke University, 2010.

[2] P. Mouroulis, R. Green, and T. Chrien. Design of pushbroom imaging spectrometers for optimum recovery of spectroscopic and spatial information. *Applied Optics*, 39:2210–2220, 2000.

[3] E. Candès, J. Romberg, and T. Tao. Robust uncertainty principles: Exact signal reconstruction from highly incomplete frequency information. *IEEE Transactions on information theory*, 52(2):489, 2006.

[4] D. Donoho. Compressed sensing. *IEEE Transactions on Information Theory*, Jan 2006.

[5] E. Candès and T. Tao. Near-optimal signal recovery from random projections and universal encoding strategies. *IEEE Trans. Information Theory*, pages 5406–5245, 2006.

[6] E. Christophe, C. Mailhes, and P. Duhamel. Hyperspectral image compression : adapting spiht and ezw to anisotropic 3-d wavelet coding. *IEEE Trans. Image Processing*, 17:2334–2346, 2008.

[7] P. Dragotti, G. Poggi, and A. Ragozini. Compression of multispectral images by three-dimensional spiht algorithm. *IEEE Trans. Geosci. Remote Sensing*, pages 416–428, 2000.

[8] A. Wagadarikar, R. John, R. Willett, and D. Brady. Single disperser design for coded aperture snapshot spectral imaging. *Applied optics*, 47(10):B44–B51, 2008.

[9] Y. Wu, I. O. Mirza, G. R. Arce, and D. W. Prather. Development of a digital-micromirror-device-based multishot snapshot spectral imaging system. *Opt. Lett*, 36:2692–2694, 2011.

[10] H. Arguello and G. R. Arce. Code aperture optimization for spectrally agile compressive imaging. *J. Opt. Soc. Am. A*, 28(11):2400–2413, Nov 2011.

[11] D. Kittle, K. Choi, A. A. Wagadarikar, and D. J. Brady. Multiframe image estimation for coded aperture snapshot spectral imagers. *Appl. Opt.*, 49(36):6824–6833, 2010.

[12] H. Arguello and G. R. Arce. Rank minimization code aperture design for spectrally selective compressive imaging. *Submitted to IEEE Transactions on Image Processing*, 2011.

[13] H. Arguello and G. R. Arce. Spectrally selective compressive imaging by matrix analysis. In *OSA Optics and Photonics Congress*, Monterey, CA, USA, 2012.

[14] R. M. Willett, R. F. Marcia, and J. M. Nichols. Compressed sensing for practical optical imaging systems: a tutorial. *Optical Engineering*, 50(7):072601, 2011.

[15] H. Arguello, H. Rueda, and G. R. Arce. Spatial super-resolution in code aperture spectral imaging. In *SPIE Conference on Defense, Security and Sensing*, Baltimore, MD, April 2012.

[16] H. Arguello, H. Rueda, and G. R. Arce. On super-resolved coded aperture spectral imaging. In *Submitted to IEEE Workshop on Signal Processing Systems*, Quebec, Canada, April 2012.

[17] H. Arguello and G. R. Arce. Restricted isometry property in coded aperture compressive spectral imaging. In *IEEE Statistical Signal Processing Workshop*, Ann Arbor, MI, USA, 2012.

[18] D. J. Brady. *Optical Imaging and Spectroscopy*. Wiley, John and Sons, 2009.

[19] M. F. Duarte and R. G. Baraniuk. Kronecker product matrices for compressive sensing. *IEEE International Conference on Acoustics Speech and Signal Processing (ICASSP)*, pages 3650–3653, 2010.

[20] M. A. T. Figueiredo, R. D. Nowak, and S. J. Wright. Gradient projection for sparse reconstruction: Application to compressed sensing and other inverse problems. *IEEE J. of Selected Topics in Signal Processing*, 1(4):586–597, 2007.